J. Fluid Mech. (2000), *vol.* 411, *pp.* 59–89. Printed in the United Kingdom

A phenomenological model for the contact region of an evaporating meniscus on a superheated slab

By S. J. S. MORRIS

Department of Mechanical Engineering, University of California, Berkeley, CA 94720, USA
e-mail: morris@me.berkeley.edu

(Received 21 October 1998 and in revised form 16 December 1999)

The evaporating meniscus of a perfectly wetting fluid exhibits an apparent contact angle Θ that is a function of superheat. Existing theory predicts Θ and the heat flow from the contact region as part of the solution of a free-boundary problem. That theory admits the possibility that much of the heat flow occurs at the nanometre scale ℓ_Θ at which Θ is determined. Here, the heat flow at that scale is proved negligible in typical applications. A phenomenological model of the contact region then holds since the part of the wetting film thinner than ℓ_Θ can be replaced by an apparent contact line. Self-consistency arguments are used to derive conditions under which (i) the phase interface can be taken as linear with assumed contact angle Θ; (ii) the heat flux to the liquid side of the phase interface is given by Newton's law of cooling with predicted heat transfer coefficient h; and (iii) the temperature satisfies Laplace's equation within the phases. When these conditions are met, prediction of the heat flow is decoupled from the physically non-trivial problem of predicting Θ. Next, this conduction theory is used to find the heat flow from the contact region of a meniscus on a conductive slab. The solution depends on Θ, the liquid–solid conductivity ratio $k = K_\ell/K_s$ and a Biot number $\mathscr{B} = hd/K_\ell$ based on slab thickness d. Asymptotic and numerical analysis is used to find the temperature in the double limit $\mathscr{B}^{-1} \to 0$ and $k \to 0$. The solution has an inner-and-outer structure, and properties of the inner region prove universal. Formulae given here for the heat flow and contact line temperature on a slab thus apply to more complex geometries. Further, the solution explains the main features seen in published simulations of evaporation from conductive solids. Near the contact line, the solid temperature varies rapidly on the scale d of the slab thickness, but varies slowly with respect to the liquid temperature. The solid temperature thus proves uniform at the scale on which Θ is determined. Lastly, the quantitative predictions of the simplified model are verified against both new and published numerical solutions of the existing theory. In typical applications, the new formulae give the heat flow and contact line temperature with an error of about 10%. This error is due to the approximations made to derive the simplified model, rather than to those made to solve it.

1. Introduction

Large heat flows occur near the intersection of a liquid–vapour phase interface with a superheated solid since the boundary temperature is nearly discontinuous there. The phase interface is almost isothermal at the saturation temperature, and the solid–fluid interface is nearly isothermal if the solid is highly conductive. If both boundaries were isothermal, the heat flux would be non-integrable at their intersection.

Small temperature variations along either boundary render the flux integrable. The mechanism of enhanced heat flow thus differs from that in convective heat transfer: there, gradients existing within a phase are enhanced by motion. A simplified model of the contact region is derived here that includes temperature variations along both interfaces. The high heat flows at the contact region are significant in heat pipes (see e.g. Stephan & Busse 1992), and in processes like spray cooling (Grissom & Wierum 1981), the spreading of volatile drops (Anderson & Davis 1995), and film dry out (Oron, Bankoff & Davis 1996). They are also important during the growth of vapour bubbles in boiling (Wilson, Davis & Bankoff 1999).

The contact region has been analysed for the stationary evaporating meniscus of a perfectly wetting system, i.e. one whose static contact angle is zero (see Potash & Wayner 1972; Moosman & Homsy 1980). That existing theory predicts the fluid and heat flow as the solution of a free-boundary problem. Though convective nonlinearities are negligible, fluid and heat flow are coupled since the flow domain is shaped by pressure differences across the phase interface. The striking prediction is qualitative. Evaporating, perfectly wetting systems should exhibit an apparent contact angle Θ caused by the pressure differences driving flow in the thin evaporating film that separates the visible meniscus from the very thin, non-evaporating wetting film. Experiments confirm this prediction (Cook, Tung & Wayner 1981, figure 4; DasGupta, Schonberg & Wayner 1993, figure 7).

Here, conditions are derived under which the only effect of hydrodynamics is to impose Θ. The heat flow is then determined by a conduction problem in which Θ is a parameter. Details of the wetting physics influence the heat flow only through the value of the phenomenological variable Θ. The existing theory then becomes a guide to formulating a relation between Θ and the superheat, rather than an essential part of predicting heat flows. This is analogous to the use of Tanner's equation in the theory of isothermal spreading. This decomposition has a general significance for evaporation problems with contact lines. Various models of the contact region occur in the literature, without discussion of when they are physically appropriate. For example, Schonberg & Wayner (1992) approximately solve the existing theory in a way that tacitly assumes significant heat flow at a dimension smaller than that on which Θ is established. By contrast, several authors assume the existence of a contact angle and analyse the conduction problem for the liquid wedge (e.g. Anderson & Davis 1994 and references in Stephan & Busse 1992). There, the heat flow is tacitly assumed negligible at dimensions smaller than those on which Θ is established. Here, conditions are derived under which the existence of a contact angle can be assumed for heat flow problems. The nanoscale modelling of Wayner and coworkers is thus related to the phenomenological approach used in the study of thick evaporating films by Davis and others.

In § 2, a self-consistency argument is used to find conditions under which the thermal singularity is smoothed over a dimension large compared with that of the region determining Θ. This separation of scales decouples the heat flow problem from that of predicting Θ. The argument is as follows. The liquid and vapour are assumed chemically identical. Fluid and heat flow are coupled in general since the local evaporative mass flux J across the liquid–vapour interface depends on the local values of the liquid and gas pressures, and on the local temperature T. Scaling is used to find conditions under which J depends only on T. The interfacial energy balance can then be written in terms of T alone, and no longer couples the thermal and flow fields. The resulting boundary condition (2) defines a heat-transfer coefficient h, and a length $L = K_\ell/h$ where K_ℓ is the liquid conductivity. L is the scale on which

conduction across the liquid balances the rate at which latent heat is absorbed at the meniscus to drive the phase change. The interface temperature proves to vary from its value at the contact line to the saturation temperature at infinity on the *adjustment* scale L. It is shown that typically $L \sim 10\,\mathrm{nm}$.

The heat flow problem proves to decouple from that of predicting Θ when (3) holds. The temperature is then determined by solving Laplace's equation in the solid and liquid, subject at the phase interface to Newton's law of cooling (2). The heat-transfer coefficient is essentially that used by Mills & Seban (1967), and more recently by Davis and coworkers (see e.g. Burelbach, Bankoff & Davis 1988, equation 2.15). In this work, a method used elsewhere in phase-change heat transfer is thus extended by proving that it can be used under specified conditions to predict the heat flux in the contact region of an evaporating wetting meniscus.

The phenomenological model is then used to find the temperature in the contact region of a meniscus on a conductive slab. This is the simplest problem to include both mechanisms essential to relax the contact line singularity. This geometry is also likely to occur in experiments. Lastly, this simple model exhibits the behaviour seen in a simulation by Stephan & Busse (1992) of evaporation from a liquid-filled groove in a highly conductive solid. Their solution exhibits a separation of length scales. Their figure 6*a* shows that the solid temperature T^s varies rapidly near the contact line. But comparison of their figure 5 with Stephan (1992, figure 5.10) shows that within the contact region, T^s is also slowly varying compared with the interface temperature. The authors neither explain this separation of scales, nor use it to interpret their results. The model problem solved here is used to explain qualitatively and quantitatively why the structure occurs.

The model problem is posed in § 3. The parameters are the contact angle Θ, liquid–solid conductivity ratio k and Biot number $\mathscr{B} = hd/K_\ell$ based on h and the slab thickness d. Numerical examples are used to show that typically $\mathscr{B}^{-1} \ll k \ll 1$. These examples are also used to motivate the choice of distinguished limit as $\mathscr{B} \to \infty$ with $k = \mathscr{T}^2/(\ln \mathscr{B})^2$ where the parameter $\mathscr{T}$ is fixed. $\mathscr{T} = \sqrt{k} \ln \mathscr{B}$ proves to control the contact line temperature T_c. In the literature, it is variously assumed that either the phase interface or substrate is isothermal. Those assumptions lead to very different predictions for the heat flow. For their case, Stephan & Busse (1992) show numerically that a model with an isothermal phase interface over-predicts the heat flow by a factor of about 3.5. The new results show when such simplifications are appropriate.

The model problem is solved in §§ 4–9. In § 4, the inner-and-outer structure for $\mathscr{B} \to \infty$ is established. In this limit, the adjustment scale $L = K_\ell/h \ll d$. Within the inner, or contact, region I the interface temperature is variable but the solid is effectively semi-infinite. Within the outer region II, the finite thickness of the slab is important, but the phase interface is isothermal at the saturation temperature.

In § 5, the contact region I is shown to have an additional substructure in the limit $k \to 0$. In region Ib, i.e. within distances of order L of the contact line, the interface temperature is variable but the highly conductive solid is isothermal to leading order in k. The solid temperature T^s thus varies slowly relative to that in the liquid. At the outer edge of region Ib, the interface temperature has adjusted to the saturation temperature. But T^s continues to vary with radial distance so that heat can flow to the contact line. There is thus a large region Ia, in which the interface temperature is uniform but T^s is variable. Most of the evaporation occurs within this large region. In § 6, T^s is found by detailed analysis of region Ia. In § 7, the problem for region Ib is solved for $0 \leqslant \Theta \leqslant \pi/2$ to determine the temperature within the liquid, and on the meniscus. Unlike the existing theory, this is not a small-slope analysis.

In § 8, the spatially integrated heat flux is found as a function of the contact line temperature T_c by forming the composite expression for the heat flows in the subregions. Here the spatially integrated flux is called the *heat flow*, for brevity. It is shown that away from the contact line, the solid sees the contact region as a line heat sink to leading order. To complete the analysis, T_c must be determined as a function of the parameters in the theory. This is done in § 9: the outer problem incorporating the slab geometry is solved there.

The main physical results are given in § 10. Definitions of the main variables are restated at the beginning of this section to make it self-contained. The main results are the formulae for the heat flow and contact line temperature. Properties of the contact region prove independent of the shape of the solid to leading order in the small parameter k. The occurrence of the slab thickness d in the Biot number $\mathscr{B}$ shows, however, that the outer geometry imposes a length scale on the inner region, and so must be incorporated in the solution. These two statements are consistent because the solution depends on $\mathscr{B}$ and k only through the parameter $\mathscr{T} = \sqrt{k}\ln\mathscr{B}$ defined above. In more complex geometries, more than one choice of d is possible. Different choices of d correspond to multiplying $\mathscr{B}$ by a numerical factor. Since this factor is of order unity, and independent of k, the value of $\mathscr{T}$ is independent of the choice of d to leading order in k. Properties of the contact region are therefore independent of the outer geometry. Results for a slab can thus be used for other geometries. This prediction is confirmed by comparison of the inner field found here for the slab with that found by Stephan & Busse (1992) for their very different geometry.

The phenomenological model is also verified in § 10 by comparison of heat flows across the meniscus on an isothermal solid. The new model is then exactly soluble. For the conditions of Stephan & Busse's study, it predicts the heat flow at a distance on 1 μm from the contact line with an error that is also about 10%. The error decreases with increasing distance. This discrepancy must be due to assumptions made in deriving the conduction model, as no approximation is made in solving it in this case.

In § 11, the asymptotic analysis of the phenomenological model is confirmed by comparison with new finite-difference solutions of it for the limiting case $\mathscr{T}^{-1} = 0$. The phase interface is then isothermal and the contact line singularity is removed by substrate conduction alone. The asymptotic state analysed in §§ 4–9 is attained for values of k occurring in practice. The discrepancy between the new results in § 10 and those of Stephan & Busse is therefore due to the assumptions made to derive the phenomenological model, rather than to the asymptotic analysis of it. This confirms the conclusion reached in § 10, and stated in the preceding paragraph. The main themes of the paper are restated in § 12.

2. Conditions under which a conduction model describes the contact region

Figure 1 shows the geometry of the contact region. The meniscus is the light curve AC. The non-evaporating wetting film mentioned in the second paragraph of § 1 is the part of AC with uniform thickness to the left of the apparent contact line O. Coupling of the fluid and heat flows is plainly important where the phase interface is curved, since the curvature is caused by a pressure difference across the interface. In this section, scaling of the Stokes equations of motion and the interfacial boundary conditions is used to determine when it is self-consistent to calculate the heat flow across the contact region by solving the conduction equation for T in the wedge

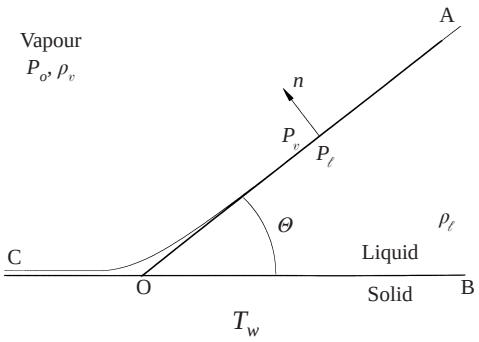

FIGURE 1. Definition sketch for the scaling analysis in § 2.

AOB, subject to Newton's law of cooling, equation (2) below, on the linear phase interface OA. The heat flow problem then decouples from that of predicting Θ.

In figure 1, P_o is the pressure in the vapour at ∞. The superheat $\Delta T = T_w - T_o$, where T_o is the saturation temperature at ∞, i.e. the temperature at which liquid and vapour coexist when both are at pressure P_o. The analysis is for vanishing superheat, i.e. $\Delta T/T_o \to 0$. Subscripts ℓ and v refer to the liquid and vapour phases.

2.1. *Simplified thermal boundary condition at the phase interface*

All heat conducted from the liquid to the interface is assumed absorbed as latent heat at the interface. This assumption holds if the kinetic energy flux, viscous power and conduction heat flux to the vapour are negligible (Burelbach *et al.* 1988, equation 2.9). It is consistent with the scaling below. Let n be distance into the vapour as shown in figure 1. Also let Q be latent heat per unit mass, and let J be the local evaporative mass flux normal to the meniscus. Then the surface energy balance is $K_\ell \partial T/\partial n + JQ = 0$.

This balance is expressed as a boundary condition on T by using the relation from kinetic theory between J and the local values of temperature T, liquid pressure P_ℓ and pressure P_v in the vapour. Let C be the sound speed in the gas. C can be assumed uniform since $\Delta T \ll T_o$. Also let $\mathscr{P}(P_\ell, T)$ be the local thermodynamic equilibrium vapour pressure, i.e. the pressure required on the vapour side of the interface for the phases to coexist at temperature T and liquid pressure P_ℓ. Lastly, let $\gamma = C_p/C_v$ be the specific heat ratio of the vapour, and let $\lambda = \sqrt{2\gamma/\pi}$. Then, by kinetic theory, $J = \lambda(\mathscr{P} - P_v)/C$. Liquid thus evaporates at a point on the interface if the local pressure P_v in the vapour is less than the pressure $\mathscr{P}$ required for coexistence.

This kinetic equation occurs in several forms in the literature. The equation above is a simplification of equation (29) in Cammenga (1980). First, the third factor on the right of his equation has been set to unity. The temperature on the interface is thus taken to equal that in the vapour. This approximation holds if $C^2/(2\gamma Q) \ll 1$. Its use introduces an error that is typically less than 5% or 6% for this paper. The same approximation is made in the existing theory of the evaporating wetting meniscus. Second, the evaporation coefficient is taken as unity following the conclusions of Cammenga (p. 377). This is also a standard assumption, see e.g. Stephan & Busse (1992, table 1). Lastly, Cammenga's (29*b*) gives exactly twice the evaporation rate predicted by the Hertz equation given as Cammenga's (11). The difference arises because Cammenga's (29*b*) takes into account that molecules have a mean motion either toward or away from the interface. Burelbach *et al.* use the Hertz equation,

so their value of the kinetic constant λ is half that above. Stephan & Busse's kinetic model is identical with that used here, with exactly the same value of λ. (We note that what Stephan & Busse call the interface temperature 'T_{iv}' is in fact the local saturation temperature, i.e. the temperature at which the phases would coexist at the local values of P_ℓ and P_v.)

The kinetic equation is simplified by expanding $\mathscr{P}(P_\ell, T)-P_v$ as a Taylor series about the reference state (P_o, T_o). To first order, $\mathscr{P}-P_o = (\rho_v/\rho_\ell)(P_\ell - P_o)+\rho_v Q(T-T_o)/T_o$ (see Guggenheim 1967, § 3.46). The linearization is valid since the coefficients, ρ_v/ρ_ℓ and $\rho_v Q/T_o$, are approximately constant over the range of $P - P_o$ and $T - T_o$ encountered in practice. The simplified expression for J is

$$\frac{JC}{\lambda} = \frac{\rho_v}{\rho_\ell}(P_\ell - P_o) - (P_v - P_o) + \rho_v Q\frac{T - T_o}{T_o}. \tag{1}$$

This kinetic equation reduces to that in the existing theory of the evaporating meniscus if $P_v = P_o$, i.e. if the pressure in the vapour is uniform. We note that the pressure terms in (1) reduce J. Fluid flows as liquid towards the contact region, evaporates and flows away as vapour. To drive these flows $P_\ell < P_o$ and $P_v > P_o$. The pressure terms thus reduce J.

Pressure terms in (1) will now be assumed negligible. Equation (1) then determines the characteristic velocities, and the momentum equation determines the pressure differences within the phases. Conditions for self-consistency are then obtained. If the pressure terms are negligible, $J \propto (T - T_o)$. The kinetic equation and energy balance then require T to satisfy Newton's law of cooling. That is

$$K_\ell \frac{\partial T}{\partial n} + h(T - T_o) = 0, \quad \text{where } h = \lambda\rho_v Q^2/(CT_o) \tag{2}$$

is the heat transfer coefficient.

2.2. *Conditions for Newton's law to hold*

Scaling will now be used to show that Newton's law holds, and that the phase interface is linear if

$$\Theta\Lambda/L \ll 1, \quad \rho_v v_\ell/(\rho_\ell CL\Theta^2) \ll 1 \quad \text{and} \quad \mu_\ell V_\ell/(\sigma\Theta^4) \ll 1. \tag{3a–c}$$

Here Λ is the molecular free path in the vapour; μ, v and σ denote the dynamic and kinematic viscosities, and surface tension; $V_\ell = (\rho_v Q\Delta T)/(\rho_\ell C T_o)$ is the characteristic liquid velocity normal to the interface: it is derived below. The length scale $L = K_\ell/h$ is defined by Newton's law (2), which implies that conduction to the interface balances the rate of absorption of latent heat at the interface on the scale L. For use in the scaling below, notice that L is a dimension perpendicular to the wall. The scale parallel to the wall is L/Θ. (See the discussion of figure 5.)

The conditions (3) have the following interpretation. Equations (3a, b) permit the use of Newton's law. First, (3a) states that pressure differences within the vapour have negligible effect on the evaporation rate at the scale L if the Knudsen number based on Λ and the vapour flow scale L/Θ is small. Next, (3b) is the condition for pressure differences within the liquid to be kinetically negligible at the scale L. Lastly (3c) ensures the phase interface is linear on the length scale L/Θ. Numerical examples below in § 2.3 show that these three conditions can hold simultaneously. These conditions will now be derived.

Velocity scales follow by balancing the left-hand side of (1) against the third term on the right. Let V_v and V_ℓ be the vapour and liquid velocities normal to the interface.

Since $J = \rho_v V_v = \rho_\ell V_\ell$, (1) requires $V_v \sim Q\Delta T/(CT_o)$ and $V_\ell \sim (\rho_v Q\Delta T)/(\rho_\ell CT_o)$. The vapour flow occurs very nearly in a half-space, and so has one length scale L/Θ. Both components of the vapour velocity thus scale as V_v. Because the liquid flow occurs in a wedge of acute angle Θ, it has two length scales L/Θ and L. By continuity, the velocity component along the wall $U_\ell \sim \Theta^{-1} V_\ell$. The ratio of inertial to viscous terms is $Re_v = \rho_v V_v L/(\mu_v \Theta)$ within the vapour, and $Re_\ell = \rho_\ell V_\ell L/\mu_\ell$ within the liquid. The numerical examples in table 1 show that both Reynolds numbers are typically less than one. The pressure difference within each phase is thus estimated by balancing the pressure gradient and viscous force per unit volume.

Pressure differences within the vapour are kinetically negligible if $\Theta\Lambda/L \ll 1$, i.e. if the continuum approximation holds within the vapour. By balancing terms in the Stokes equation, we find that a pressure difference $P_v - P_o \sim \Theta\mu_v V_v/L$ is needed to drive the vapour flow. The definition of V_v implies that the third term on the right of (1) is of order $\rho_v CV_v$. The ratio of the gas pressure term in (1) to the thermal term is thus $(P_v - P_o)/(\rho_v V_v C) \sim \Theta v_v/(CL)$. But by kinetic theory $v_v \sim C\Lambda$. Condition (3*a*) is established.

Next, pressure differences within the liquid are negligible if $\rho_v v_\ell/(\rho_\ell CL\Theta^2) \ll 1$. By balancing terms in the lubrication equation for the thin liquid film, we find that $P_o - P_\ell \sim \mu_\ell V_\ell/(L\Theta^2)$. The relation $U_\ell \sim V_\ell/\Theta$ has been used, and so has the remark about length scales above. The ratio of the liquid-pressure term in (1) to the thermal term is thus $(P_o - P_\ell)/(\rho_\ell CV_v) \sim \rho_v v_\ell/(\rho_\ell CL\Theta^2)$. Condition (3*b*) is established.

Lastly, the phase interface can be taken as linear if $\mu_l V_l/(\sigma\Theta^4) \ll 1$. This is proved by estimating the change $\Delta\Theta$ in angle over the length scale L/Θ. $\Delta\Theta$ is determined by the normal component of the interfacial momentum balance. For that balance, see Burelbach *et al.* (1988, equation 2.10). Because $Re \ll 1$ within each phase, the interfacial momentum balance reduces to a normal stress balance. The pressure is at least comparable to the normal viscous stress in creeping flow, and exceeds it in the lubrication approximation. To estimate $\Delta\Theta$, it suffices to balance the pressure difference across the interface against the surface tension force normal to it. So $P_g - P_\ell \sim \sigma \mathrm{d}\Theta/\mathrm{d}s$ where s is length along the interface. In distance L/Θ, the change in Θ is $\Delta\Theta \sim (P_v - P_\ell)L/(\sigma\Theta)$. For the examples in table 1, $P_v - P_\ell$ can be approximated by $P_o - P_\ell \sim \mu_\ell V_\ell/(L\Theta^2)$. So $\Delta\Theta/\Theta \sim \mu_\ell V_\ell/(\sigma\Theta^4)$. Condition (3*c*) is established.

2.3. *Numerical examples*

Table 1 shows numerical estimates for some examples described in the literature. For columns 1–3, see respectively Schonberg *et al.* (1995; table 1, case 2), DasGupta *et al.* (1993, table 1; also figure 7, curve 3) and Stephan & Busse (1992, table 1). For simplicity, the kinetic constant $\lambda = 1$ for these examples. Material properties are given in books on heat pipes. Subscript M denotes a velocity induced by the Marangoni effect. The table shows that both Reynolds numbers are typically less than one, as assumed above.

The table shows that conditions (3*a–c*) can hold simultaneously. If taken literally, the scaling would also imply that the phenomenological theory holds for the examples in columns 1 and 3. Use of the theory for the example in column 2 would, however, be marginal by that reasoning. That conclusion is unduly conservative. Scaling gives no information about how small a dimensionless parameter should be for an approximation to hold. In a subsequent work (Morris 2000), the phenomenological theory is derived by asymptotic analysis of the existing theory for the case of an isothermal substrate. The approach to the asymptotic state can thus be studied. Application of those results here would show that the phenomenological theory describes all three cases.

	C_7H_{16}/Si	C_7H_{16}/Si	NH_3/Al
T_o (K)	373	373	300
$\Delta T = T_w - T_o$ (K)	5.2	0.0008	1.3
Θ(rad)	~ 0.4	0.025 ± 0.02	~ 0.3
Source for Θ:	Schonberg *et al.* (1995) computed	DasGupta *et al.* (1993) measured	Stephan & Busse (1992) computed
$L = K_\ell/h$ (nm)	20	20	5
$Re_v = \rho_v V_v L/(\mu_v \Theta)$	0.6	0.002	0.2
$Re_\ell = \rho_\ell V_\ell L/\mu_\ell$	0.09	2×10^{-6}	0.004
(3*a*): $\Theta \Lambda/L$	0.2	0.01	0.09
(3*b*): $\rho_v v_\ell/(\rho_\ell C L \Theta^2)$	0.003	0.9	0.02
(3*c*): $\mu_\ell V_\ell/(\sigma \Theta^4)$	0.009	1	0.1
$V_{\ell M}/V_\ell$	0.6	0.002	0.2
V_{vM}/V_v	0.6	0.6	0.4

TABLE 1. Flow scales for perfectly wetting systems.

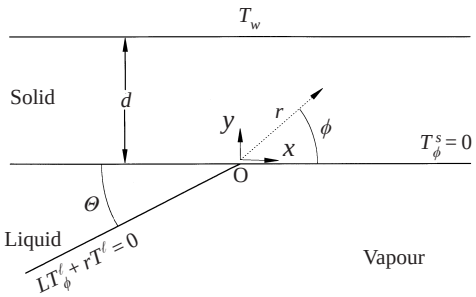

FIGURE 2. Definition sketch for the conduction model (4) of an evaporating meniscus on a conducting slab.

The final rows in table 1 show the ratio of the Marangoni velocity to that due to evaporation. In this paragraph only, T_c is the critical temperature of the fluid. The Marangoni stress, i.e. the gradient of σ along the phase interface, is of order $\Theta \sigma \Delta T/(LT_c)$. The relation $\mathrm{d}\sigma/\mathrm{d}T \sim \sigma/T_c$ has been used: for it, see Guggenheim (1967, § 3.65). By balancing the Marangoni and viscous stresses, the velocity along the wall $U_{\ell M} \sim \Theta \sigma \Delta T/(\mu_\ell T_c)$. So $V_{\ell M}/V_\ell \sim \rho_\ell \sigma C T_o \Theta^2/(\rho_v \mu_\ell Q T_c)$, since $V_{\ell M} \sim \Theta U_{\ell M}$. Similarly, $V_{vM}/V_v \sim \sigma C T_o/(\mu_v Q T_c)$. Table 1 suggests the Marangoni effect is not an issue, if the fluid is pure.

Lastly, table 1 shows that $Re_l \ll 1$. Since the Prandtl number is of order unity for the liquids of interest, the Péclet number is also small. So when (3) holds, the heat flow is found by solving Laplace's equation for T subject to Newton's law of cooling on a linear phase interface with prescribed contact angle Θ. This phenomenological model is applied to the title problem in the rest of this work.

3. Boundary-value problem

Let $\Delta T = T_w - T_o$, as defined in § 2. Define dimensionless variables (without stars) by $T_* = T_o + T\Delta T$ and $(x, y)_* = (x, y)L$. Here $L = K_\ell/h$ is the adjustment scale defined following (3). The Biot number $\mathscr{B} = hd/K_\ell$, as defined in § 1. $\mathscr{B}$ is the ratio of slab thickness to adjustment scale.

Figure 2 shows the geometry. As shown there, (r, ϕ) are polar coordinates with ϕ measured through the solid from the solid–vapour interface. The phase interface is taken as linear to analyse the contact region because the scale L of this region is small compared with the radius of curvature of the visible meniscus. Superscripts v, ℓ and s refer respectively to the vapour, liquid and solid. Superscript f refers to either fluid phase.

Then, within the liquid and solid

$$T_{xx} + T_{yy} = 0; \quad \text{at } y = \mathscr{B}, \quad T = 1; \quad \text{at } \phi = 0, \quad T^s_\phi = 0;$$
$$\text{at } \phi = \pi + \Theta, \quad T^\ell_\phi + rT^\ell = 0; \tag{4a–d}$$
$$\text{at } \phi = \pi, \quad T^s = T^\ell \quad \text{and} \quad T^s_\phi = kT^\ell_\phi. \tag{4e,f}$$

In (4*a*), the solid is assumed to conduct isotropically. This is so even for single crystals if the structure is cubic, as it is for silicon and aluminium. Boundary conditions (4*b*, *c*, *d*) state the following. The top $y = \mathscr{B}$ of the slab is isothermal; the solid sees the solid–vapour interface as adiabatic because the conductivity of the vapour is negligible; and Newton's law of cooling (2) applies at the liquid–vapour interface. Boundary conditions (4*e*,*f*) state that the temperature and heat flux are continuous at the solid–liquid interface.

Heat leaves the solid only across the solid–liquid interface $\phi = \pi$ by (4*c*). The dimensional rate q_* at which heat flows across the interval $(0, r)$ of this axis is given by

$$q_*/(K_\ell \Delta T) = \int_{-\infty}^{\xi} T^\ell_\phi \, \mathrm{d}\xi, \quad \text{where } \xi = \ln r. \tag{5}$$

In (5), the gradient T^ℓ_ϕ is calculated on the liquid side of the solid–liquid interface. The left-hand side of (5) is dimensionless, since q_* has units of power per unit length of contact line.

For later use, we note that q_* grows as $\ln r$ as $r \to \infty$. By Newton's law of cooling (4*d*), the interface temperature $T \to 0$ as $r \to \infty$. But within the solid, $T \to 1$ as $r \to \infty$ since the flux from the solid vanishes asymptotically as the liquid layer becomes increasingly thick. So the liquid is bounded asymptotically by the isotherms 0, 1 and $T^\ell_\phi \to \Theta^{-1}$. By (5),

$$\Theta q_*/(K_\ell \Delta T) \sim \ln r \quad \text{as } r \to \infty \text{ with } k \text{ and } \mathscr{B} \text{ fixed.} \tag{6}$$

Table 2 shows estimates of the control parameters. $\mathscr{B}$ is calculated for slab thickness $d = 1\,\text{mm}$ and kinetic constant $\lambda = 1$. For perfectly wetting systems, estimates of the apparent contact angle Θ are given in table 1 above. For water on stainless steel, the static contact angle $\Theta \sim 0.7$ radians (Bankoff 1994). Table 2 shows that typically $\mathscr{B}^{-1} \ll k \ll 1$. Because $\mathscr{B}^{-1} \ll 1$, $L \ll d$ and the solution has an inner-and-outer structure. Though both $\mathscr{B}^{-1}$ and k are small, the parameter

$$\mathscr{T} = k^{1/2} \ln \mathscr{B} \tag{7}$$

is of order unity. $\mathscr{T}$ proves to determine the temperature at the contact line, as shown by (32).

In §§ 4–9, problem (4) is solved for $\mathscr{B} \to \infty$ with $\mathscr{T}$ fixed. Because $d \gg L$, the phase interface is asymptotically isothermal far from the contact line. Because k is logarithmically small in $\mathscr{B}$, the solid is a good conductor compared with the liquid. The solution includes as special cases the extremes in which the phase interface or solid is isothermal. The phase interface is isothermal if negligible superheat is needed

	T_o (K)	$\mathscr{B}/10^5$	$100k$	$\mathscr{T}$
NH_3/Al	300	2	0.2	0.5
C_7H_{16}/Si	373	0.5	0.1	0.3
H_2O/st. steel	373	0.3	5	2

TABLE 2. Estimates of the control parameters.

to drive evaporation from it. This is so if $h \to \infty$ with all else fixed, i.e. if $\mathscr{T} \to \infty$. The solid is isothermal if negligible temperature difference is needed to drive heat to the liquid. This is so if $k \to 0$ with all else fixed, i.e. if $\mathscr{T} \to 0$. The extremes correspond respectively to either the interface or solid having negligible thermal resistance.

4. Inner-and-outer structure of problem (4) for $\mathscr{B} \to \infty$ with $\mathscr{T}$ fixed

In this limit, terms of order $k = (\mathscr{T}/\ln \mathscr{B})^2$ are logarithmically small in $\mathscr{B}$. They are kept in the problem in this section since all logarithmically small terms are formally larger than any algebraically small correction. So we first discuss the structure caused by the limit $\mathscr{B} \to \infty$, and then add that due to the limit $k \to 0$.

The inner limit is $\mathscr{B} \to \infty$ with r fixed. This limit defines the contact region I. Since distance is measured in units of L, the top $y = \mathscr{B}$ of the slab moves to ∞ as $\mathscr{B} \to \infty$. Boundary condition (4b) is thus replaced by a matching condition at ∞. The inner problem is otherwise identical to (4). It is

$$r(rT_r)_r + T_{\phi\phi} = 0 \quad \text{in both liquid and solid;} \tag{8a}$$

$$\text{at } \phi = 0,\ T^s_\phi = 0; \quad \text{at } \phi = \pi,\ T^s = T^\ell \quad \text{and} \quad T^s_\phi = kT^\ell_\phi;$$

$$\text{at } \phi = \pi + \Theta,\ T^\ell_\phi + rT^\ell = 0. \tag{8b–e}$$

For the outer problem, distance is measured in units of d, so that the outer coordinate $\bar{r} = r/\mathscr{B}$. The outer limit is $\mathscr{B} \to \infty$ with fixed $\bar{r} \neq 0$. This limit defines the outer region II. Newton's law (4d) is exactly $T^\ell_\phi + \mathscr{B}\bar{r}\,T^\ell = 0$. In the outer limit, this simplifies to $T^\ell = 0$: the interface temperature is then fixed at the saturation temperature. In region II, the temperature difference needed to drive evaporation is negligibly small since $\mathscr{B} \to \infty$ corresponds to $h \to \infty$. The outer problem is otherwise identical to (4). It is

$$\bar{r}(\bar{r}T_{\bar{r}})_{\bar{r}} + T_{\phi\phi} = 0 \quad \text{in both liquid and solid;} \tag{9a}$$

$$\text{at } \phi = 0,\ T^s_\phi = 0; \quad \text{at } \phi = \pi,\ T^s = T^\ell \quad \text{and} \quad T^s_\phi = kT^\ell_\phi;$$

$$\text{at } \phi = \pi + \Theta,\ T^\ell = 0; \quad \text{at } \bar{y} = 1,\ T = 1. \tag{9b–f}$$

Solutions of (8) and (9) can be matched as the interface conditions (8e) and (9e) are equivalent for $r \gg 1$.

In the older heat pipe literature, the entire meniscus is modelled by problem (9). The heat flux is thus made integrable by substrate conduction. For a particular case, Stephan & Busse (1992) show that those models greatly over-estimate the heat flow. The structure of the present analysis already shows that this will be so: in the distinguished limit analysed here, the maximum heat flux is determined by problem (8) for the contact region, not the outer problem (9) in which the interface is taken

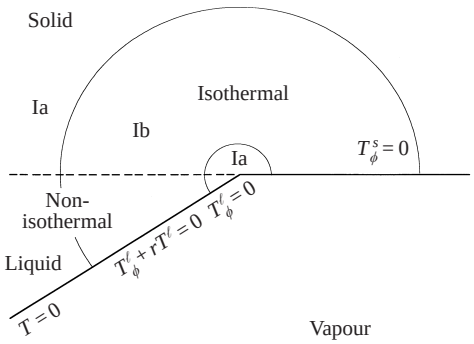

FIGURE 3. Effect of vanishing liquid–solid conductivity ratio on the structure of the contact region. As discussed in the text, the isotherms are approximately radial within the liquid, and circular within the solid.

as isothermal. The heat flow is thus controlled by kinetics rather than by substrate conduction.

5. Effect of vanishing conductivity ratio on the contact region I

Figure 3 shows the structure of the contact region I to be established here. For $k \to 0$, the contact region subdivides into an outer region Ia and an inner region Ib. Within region Ia, r is either exponentially small in k or exponentially large in k. Newton's law (8*e*) thus reduces to $T_\phi = 0$ within the inner circle in the figure, and to $T = 0$ outside the large circle. Within region Ib, $r = O(1)$ and Newton's law does not simplify.

The qualitative behaviour of the temperature field can be understood as follows. Newton's law imposes a length scale on T^ℓ, which thus varies over dimensionless distances $O(1)$. But in the highly conductive solid, T varies slowly with respect to position. T^s thus proves uniform within the large circle in figure 3, and varies significantly only when r is large, i.e. outside the large circle. Since the heat flux to the phase interface is greatest for $r = O(1)$, heat flows within the solid purely radially at leading order in k. So the isotherms are approximately circular within the solid.

Things are different within the liquid. Outside the large circle, Newton's law requires only that $T = 0$ on the interface. Far from the contact line, T^ℓ thus varies slowly with radial distance. The variation is driven by that in the solid. The isotherms, however, are approximately radial within the liquid since heat flows across the liquid to the interface. Next, in the liquid part of the annulus Ib, T^ℓ varies over distances $O(1)$. Both radial and azimuthal conduction are important as the isotherms turn towards the solid to drive heat to the inner region of the meniscus. In region Ib, we find that T^ℓ satisfies the full Laplace equation. Lastly, within the liquid part of the small circle, r is exponentially small in k. Newton's law reduces to a no-flux condition. Like the solid, the liquid is isothermal within this small region.

The scaling used to construct the solution of (8) will now be motivated, and then shown to lead to a self-consistent solution. Consider the temperature outside the large circle shown in figure 3. Formally, this is the outer limit of the inner problem (8). Newton's law (8*c*) then reduces to $T^\ell = 0$ on the interface, as shown in figure 3. The problem consisting of (8*a–d*) with this simplified interface condition admits the

separable solution

$$T^s = r^p \frac{\cos p\phi}{\cos p\pi} \quad \text{and} \quad T^\ell = r^p \frac{\sin p(\pi + \Theta - \phi)}{\sin p\Theta}, \quad \text{where } \tan p\pi \tan p\Theta = k. \tag{10a–c}$$

This solution is derived in another context by Anderson & Davis (1994, equation 3.4). The separation constant p is determined by (10c), whose roots are countably infinite.

The smallest positive root of (10c) is of special interest. The solution of the outer problem (9) must match to the solution of (8) as the outer coordinate $\bar{r} \to 0$. The inner limit $\bar{r} \to 0$ of the outer solution is controlled by the most singular of the modes (10), i.e. by the smallest positive root of (10c). Let

$$\alpha = 1/\sqrt{\pi\Theta} \quad \text{and} \quad \tilde{\xi} = \sqrt{k} \ln r, \text{ so } r = \exp(\tilde{\xi}/\sqrt{k}). \tag{11}$$

Then for $k \to 0$, the smallest positive root of (10c) is given by $p \sim \alpha\sqrt{k}$. The most singular mode remaining finite as $\bar{r} \to 0$ is thus $T \propto r^p \propto \exp(\alpha\tilde{\xi})$.

Derivatives in $\tilde{\xi}$ are therefore of order unity in the overlap region between the contact region I and the outer region II. This suggests the use of $\tilde{\xi}$ as a coordinate. Derivatives in $\tilde{\xi}$ prove of order unity throughout the solid. T^s is thus uniform on the inner scale L, as discussed above. But T^ℓ varies even on the scale L since Newton's law forces the interface temperature to vary on this scale. These variations in T^ℓ resolve the thermal singularity. Since information about the interface temperature is transmitted to the highly conductive solid only through the liquid, T^s varies more slowly with position than does T^ℓ. Because derivatives of T^ℓ are finite, the length scale for T^s can be set by the outer problem (9) in which the meniscus temperature $T = 0$.

The scaling $p \sim \alpha\sqrt{k}$ is central to this work, so we explain it. Because the solid–vapour interface is adiabatic, T^s is an even function of ϕ. The gradient at the solid–liquid interface thus scales as p^2, and continuity of the flux requires $p^2 \propto k/\Theta$. So $p \sim \alpha\sqrt{k}$.

The structure shown in figure 3 can now be established. When expressed in terms of $\tilde{\xi}$, the inner problem (8) becomes without approximation,

$$k T_{\tilde{\xi}\tilde{\xi}} + T_{\phi\phi} = 0 \quad \text{in both liquid and solid;} \tag{12a}$$

$$\text{at } \phi = 0,\ T^s_\phi = 0; \quad \text{at } \phi = \pi,\ T^s = T^\ell \quad \text{and} \quad T^s_\phi = k T^\ell_\phi;$$

$$\text{at } \phi = \pi + \Theta,\ T^\ell_\phi + T^\ell \exp(\tilde{\xi}/\sqrt{k}) = 0. \tag{12b–e}$$

Where derivatives in $\tilde{\xi}$ are $O(1)$, (12a) reduces at leading order to $T_{\phi\phi} = 0$. This allows the isotherms to be circular within the solid, and radial within the liquid as claimed above in the discussion of figure 3.

6. Temperature within the outer contact region Ia

T^s is determined by the region Ia shown in figure 3. This region is defined by the limit $k \to 0$ with fixed $\tilde{\xi} \neq 0$. Within it, $r = \exp(\tilde{\xi}/k^{1/2})$ is either exponentially small, or large, in k according as $\tilde{\xi}$ is negative or positive. With exponentially small error in k, (12) is therefore equivalent to the following problem:

$$k T_{\tilde{\xi}\tilde{\xi}} + T_{\phi\phi} = 0 \quad \text{in both liquid and solid;} \tag{13a}$$

$$\text{on } \phi = 0,\ T^s_\phi = 0; \quad \text{at} \quad \phi = \pi,\ T^s = T^\ell \quad \text{and} \quad T^s_\phi = k T^\ell_\phi;$$

$$\text{on } \phi = \pi + \Theta,\ 0 = \begin{cases} T^\ell_{0\phi} & \text{if } \tilde{\xi} < 0 \\ T^\ell_0 & \text{if } \tilde{\xi} > 0. \end{cases} \tag{13b–e}$$

By (13*b*) the solid–vapour interface appears adiabatic to the solid. By (13*e*), the phase interface is effectively adiabatic near the contact line (i.e. for $\tilde{\xi} < 0$) and isothermal far from the contact line (i.e. for $\tilde{\xi} > 0$). In figure 3, these regions correspond to the interior of the small circle, and the exterior of the small circle.

The solution of (13) takes the form

$$T = T_0(\tilde{\xi}, \phi) + k^{1/2}\, T_1(\tilde{\xi}, \phi) + k\, T_2(\tilde{\xi}, \phi) + k^{3/2}\, T_3(\tilde{\xi}, \phi) + O(k^2). \tag{14}$$

Odd integer powers of $k^{1/2}$ are required here for matching to the solution in the outer region II. Boundary-value problems for the coefficients $T_0, T_1, \ldots$ are obtained by substituting (14) into (13), and equating to zero the coefficients of the gauge functions $1,\ k^{1/2}, \ldots$.

6.1. *Solution for* T_0 *and* T_1

In both liquid and solid, $T_{0\phi\phi} = 0$. The boundary conditions are as follows:

$$\text{at } \phi = 0,\ T^s_{0\phi} = 0; \quad \text{at } \phi = \pi,\ T^s_0 = T^\ell_0 \quad \text{and} \quad T^s_{0\phi} = 0;$$
$$\text{at } \phi = \pi + \Theta, \quad 0 = \begin{cases} T^\ell_{0\phi} & \text{if } \tilde{\xi} < 0 \\ T^\ell_0 & \text{if } \tilde{\xi} > 0. \end{cases} \tag{15a–d}$$

These boundary conditions differ from those in (13) only because (15*c*) shows that the liquid–solid interface appears adiabatic to the solid at leading order.

The solution of $T_{0\phi\phi} = 0$ subject to (15) is

$$T^s_0 = A_0(\tilde{\xi}) \quad \text{and} \quad T^\ell_0 = \begin{cases} A_0(\tilde{\xi}) & \text{if } \tilde{\xi} < 0 \\ (\pi + \Theta - \phi)A_0(\tilde{\xi})/\Theta & \text{if } \tilde{\xi} > 0. \end{cases} \tag{16}$$

The function of integration $A_0(\tilde{\xi})$ is determined at $O(k)$. See § 6.2 below.

The solution for the solid has the following interpretation. By (15*a*, *c*), the entire solid–fluid interface is adiabatic at this order. The field equation $T_{0\phi\phi} = 0$ then allows T_0 to depend only on r. Since heat is conducted to the contact line through the solid, the isotherms in the inner region I of the solid are circular to leading order. This is as claimed in the discussion of figure 3 above. The circular isotherms can be seen in figure 7 of Stephan & Busse (1992).

Within the liquid, the behaviour of (16) is more complex. Near the contact line, Newton's law requires $T^\ell_\phi \to 0$ at the phase interface, as in the first case of (15*d*). The field equation $T_{0\phi\phi} = 0$ then allows T_0 to depend only on r, as in the solid. But far from the contact line, Newton's law requires $T \to 0$. The field equation then requires T_0 to fall linearly with ϕ from the solid–liquid interface to the liquid–vapour interface. This allows heat conduction from the solid to the evaporating meniscus. Because A_0 is a slowly varying function of r, the isotherms are nearly rays in the outer limit of the inner solution. This too can be seen in the numerical simulations of Stephan & Busse.

T^s can be made continuous at $\tilde{\xi} = 0$ by choosing A_0 to be continuous there. This is not so for T^ℓ. On the interface $\phi = \pi + \Theta$, and (16) shows that T^ℓ jumps from $A_0(0)$ for $\tilde{\xi} = 0^-$ to zero for $\tilde{\xi} > 0$. This discontinuity has the following interpretation. The problem is described using the variable $\tilde{\xi}$ because $\partial T/\partial\tilde{\xi}$ is of order unity within the solid. But in terms of this variable, T^ℓ varies smoothly except at $\tilde{\xi} = 0$. There, the variation is rapid compared with that in the solid. Physically, conduction through the highly conductive solid elevates the interface temperature near the contact line above the saturation temperature $T = 0$. The temperature within the liquid varies on the scale L imposed by Newton's law of cooling. This scale is independent of k,

so T^{ℓ} appears discontinuous when plotted in terms of the stretched variable $\tilde{\xi}$. The temperature variation on the fast scale L is found in § 7 by analysing the innermost region Ib.

T_1 and T_0 satisfy the same boundary-value problem, as (13) involves only the first power of k. The solution for T_1 is the same as that for T_0 but with $A_0(\tilde{\xi})$ replaced by a second arbitrary function $A_1(\tilde{\xi})$. This function is determined at $O(k^{3/2})$.

6.2. *Solution for T_2^s and A_0*

T_2^s satisfies

$$T^s_{2\phi\phi} + A_0''(\tilde{\xi}) = 0; \quad \text{at } \phi = 0,\ T^s_{2\phi} = 0; \quad \text{at } \phi = \pi,\ T^s_{2\phi} = \begin{cases} 0 & \text{if } \tilde{\xi} < 0 \\ -A_0/\Theta & \text{if } \tilde{\xi} > 0. \end{cases} \tag{17a–c}$$

This problem determines A_0, and so the temperature within both the liquid and solid. The important boundary condition is (17c). It shows that the solid–liquid interface appears adiabatic for $\tilde{\xi} < 0$, i.e. at distances from the contact line that are exponentially small in $\sqrt{k}$. But for $\tilde{\xi} > 0$, the solid loses heat to the liquid at a rate set by A_0. Since (17a) requires the temperature gradient within the solid to vary linearly with $A_0''(\tilde{\xi})$, (17) determines the function A_0.

The solution of (17a) satisfying (17b) is $T_2^s = A_2(\tilde{\xi}) - \frac{1}{2}A_0''(\tilde{\xi})\phi^2$. $A_0(\tilde{\xi})$ is determined by imposing (17c). A_0 thus satisfies

$$A_0'' = 0 \text{ for } \tilde{\xi} < 0 \quad \text{and} \quad A_0'' = \alpha^2 A_0 \text{ for } \tilde{\xi} > 0. \tag{18a, b}$$

Here $\alpha = 1/\sqrt{\pi\Theta}$, as defined by (11) above. By proceeding to $O(k^{3/2})$ we find that A_1 also satisfies (18). $A_0(\tilde{\xi})$ and $A_1(\tilde{\xi})$ are determined by (18), and the condition that both (A_0, A_1) and the derivatives (A_0', A_1') be continuous at $\tilde{\xi} = 0$. It makes sense that the r-dependence of T is determined by the solid. Within the non-trivial part of region Ia, the interface temperature $T^{\ell v} = 0$. If the solid were isothermal, T^{ℓ} would therefore depend only on ϕ.

6.3. *Solid temperature and heat flow in region Ia*

T^s is found by solving (18) to determine T_0 and T_1. Let $\mathscr{H}(\tilde{\xi})$ be the Heaviside unit function. Also let $c_0(\mathscr{T})$ and $c_1(\mathscr{T})$ be arbitrary functions of $\mathscr{T}$. These functions are determined by matching to the outer problem in § 9. Then, by solving (18)

$$T^s/T_c = 1 + (\cosh\alpha\tilde{\xi} - 1)\mathscr{H}(\tilde{\xi}), \quad \text{where } T_c = c_0(\mathscr{T}) + k^{1/2}c_1(\mathscr{T}) \tag{19a, b}$$

is the temperature at the contact line, i.e. as $\tilde{\xi} \to -\infty$. The isotherms within the solid are thus circular at this order, as claimed in the discussion of figure 3. They become non-circular at $O(k)$ to allow heat flow into the liquid, as shown by the solution for T_2 preceding (18).

The solution for T^s can be interpreted as follows. The temperature in the highly conductive solid varies slowly compared with the temperature in the liquid. The boundary conditions seen by the solid at the solid–liquid interface are therefore $T^s_{\phi} = 0$ for $r < 1$ and $T^s_{\phi} = -k\Theta^{-1}T^s$ for $r > 1$. The second equation is simply the flux continuity condition at the solid–liquid interface: the gradient in the liquid is evaluated as $(T^s - T^{\ell v})/\Theta$ and the interface temperature $T^{\ell v}$ is taken as zero. Laplace's equation can be solved separately for $r < 1$ and $r > 1$, and the solutions joined by requiring both T and T_r to be continuous on the semicircle $r = 1$. The

solution for T^s is thus

$$T^s/T_c = \begin{cases} \frac{1}{2}(r^p + r^{-p})\cos p\phi & \text{if } r > 1 \\ 1 & \text{if } r \leqslant 1. \end{cases}$$

Here T_c is the (unknown) temperature at the contact line $r = 0$ and $p \sim \alpha\sqrt{k}$, as defined following (11). Equation (19) is the expansion correct to $O(p)$ of this expression. This argument shows that T^s varies as $\cosh \alpha\tilde{\xi}$ because the solid sees a flux $k\Theta^{-1}T^s$ into the liquid for $r > 1$.

The outer limit of (19) is needed later for matching to the outer solution defined by (9). It follows by using the identity $\tilde{\xi} = \mathscr{T} + \sqrt{k}\ln\bar{r}$ to express (19) in terms of the outer variable $\bar{r}$, and then applying the outer limit $k \to 0$ with $\bar{r}$ fixed. This procedure is equivalent to the definition of the outer limit given in §4 since $k \to 0$ in the limit $\mathscr{B} \to \infty$ with $\mathscr{T}$ fixed. Thus

$$T^s/(c_0 \cosh \alpha\mathscr{T}) = 1 + k^{1/2}\left(\frac{c_1}{c_0} + \alpha \tanh \alpha\mathscr{T}\ \ln\bar{r}\right) + O(k). \tag{20}$$

This expression holds within the solid for fixed $\bar{r} \ll 1$, as it is derived from the solution of the inner problem (8). It shows that to a first approximation, T^s is uniform far from the contact line. At second order, T^s varies with $\bar{r}$ to allow conduction to the contact line. Since this variation is logarithmic in $\bar{r}$, the distant solid sees the contact region as a line heat sink.

The dimensional heat flow q^*_{Ia} to the liquid through region Ia can be found by using (19) to calculate the radial heat flow within the solid across a semicircle of arbitrary radius r, i.e. $k^{-1}\pi r T^s_r$. The heat flow to the liquid for $\tilde{\xi} > 0$ is thus given by

$$\Theta q^*_{\mathrm{Ia}}/(K_\ell \Delta T) = T_c \frac{\sinh \alpha\tilde{\xi}}{\alpha\sqrt{k}} + o(1). \tag{21a}$$

The heat flow vanishes at $\tilde{\xi} = 0$ as the meniscus is effectively adiabatic near the contact line. Equation (21) gives the contribution of region Ia to the heat flow with error $o(1)$. This is, in effect, the heat flow across the part of the meniscus for which $T^{\ell v}$ can be taken as uniform, since in Ia the liquid–vapour interface is either adiabatic or isothermal by (13*e*). The equation can be interpreted by using the identity $\tilde{\xi} = \sqrt{k}\ln r$ to express it in terms of r. This gives

$$\Theta q^*_{\mathrm{Ia}}/(K_\ell \Delta T) = T_c \frac{r^{\alpha\sqrt{k}} - r^{-\alpha\sqrt{k}}}{2\alpha\sqrt{k}} \quad \text{for } r \geqslant 1. \tag{21b}$$

If the wall temperature were uniform, the heat flow would vary as $\ln r$ as $r \to \infty$, as in (6). The dependence in (21) is more complicated because T^s varies slowly in r on the solid–fluid interface.

Equation (21) does not give the total rate at which heat flows across the contact region. An additional amount of order $K_\ell \Delta T$ flows across region Ib, in which the meniscus temperature is variable. That contribution is larger than the error in (21), and so is found next.

7. Temperature within the inner contact region Ib

The inner contact region Ib is shown as an annulus in figure 3. This region is defined formally by taking the limit $k \to 0$ with $\tilde{\xi}/k^{1/2}$ fixed. Within it, $T^{\ell v}$ proves to vary smoothly from the saturation temperature at ∞ to the contact line temperature

T_c. In scaling the Laplace equation (12), $T_{\tilde{\xi}\tilde{\xi}}$ is assumed of order unity. Within the solid, the method is self-consistent as A'' is discontinuous but finite at $\tilde{\xi} = 0$. But as discussed above (17), the method is locally inconsistent for the liquid because T^ℓ proves discontinuous at $\tilde{\xi} = 0$. Physically, Newton's law of cooling forces both $T^{\ell v}$ and T^ℓ to vary on the scale L near the contact line. The temperature variation on this scale is determined in this section. Formally, T^ℓ is made continuous by inserting an interior layer at $\tilde{\xi} = 0$.

Let $\xi = \tilde{\xi}/k^{1/2}$ so $r = \exp\xi$, as defined by (5). Also let $T = \hat{T}_0 + O(k^{1/2})$. The equation for $\hat{T}_0$ follows by expressing the inner problem (8) in terms of ξ and applying the limit $k \to 0$. So

$$\hat{T}_{0\xi\xi} + \hat{T}_{0\phi\phi} = 0 \quad \text{in both liquid and solid}; \tag{22a}$$

$$\text{at } \phi = 0 \text{ and at } \phi = \pi,\ \hat{T}^s_{0\phi} = 0; \quad \text{at } \phi = \pi,\ \hat{T}^s_0 = \hat{T}^\ell_0;$$

$$\text{at } \phi = \pi + \Theta,\ \hat{T}^\ell_{0\phi} + \mathrm{e}^\xi \hat{T}^\ell_0 = 0. \tag{22b–e}$$

The matching conditions within the liquid are that $\hat{T}^\ell \to c_0$ as $\xi \to -\infty$ and $\hat{T}^\ell \to c_0(\pi + \Theta - \phi)/\Theta$ as $\xi \to \infty$. Within the solid, $\hat{T}^s \to c_0$ as $|\xi| \to \infty$. These conditions are explained below, where they are used.

Boundary conditions (22*b–e*) have the following interpretation. The entire fluid–solid interface appears adiabatic to the solid within this region by (22*b*, *c*). Also the meniscus boundary condition (22*e*) varies smoothly from the no-flux condition $\hat{T}^\ell_{0\phi} = 0$ at $-\infty$ to the isothermal condition $\hat{T}^\ell_0 = 0$ at $+\infty$.

The solid temperature $\hat{T}^s$ is uniform within this region, and equal to the contact line temperature T_c. This follows as all boundaries of this region are adiabatic. By (22*b*, *c*), the fluid–solid interface is adiabatic. $\hat{T}^s_0$ is thus determined by the boundary conditions as $|\xi| \to \infty$. Since the solution (19) in region Ia is continuous to $O(k^{1/2})$, matching requires $\hat{T}^s_0 \to c_0$ as $|\xi| \to \infty$. This is the matching condition stated above. The solution of (22*a*) subject to these conditions and (22*b*) is $\hat{T}^s_0 = c_0$. The solid is therefore isothermal.

$\hat{T}^\ell_0$ can now be found. Let $u(\xi, \phi)$ satisfy

$$u_{\xi\xi} + u_{\phi\phi} = 0 \quad \text{for} \quad \pi < \phi < \pi + \Theta; \quad \text{on } \phi = \pi,\ u = 1;$$

$$\text{on } \phi = \pi + \Theta,\ u_\phi + \mathrm{e}^\xi u = 0. \tag{23a–c}$$

By comparison with (22), $\hat{T}^\ell_0 = c_0 u$. Physically, (23) describes conduction across a liquid wedge on an isothermal solid with Newton's law of cooling applied at the phase interface. Because T^s varies slowly compared with T^ℓ, the temperature on the solid–fluid interface equals the first approximation $c_0(\mathscr{T})$ to the contact line temperature.

The most interesting aspect of (23) is the behaviour it predicts for total heat flow across region Ib. Far from the contact line, (23*c*) reduces to $u = 0$ so that $u \to (\pi + \Theta - \phi)/\Theta$. The dimensional heat flow q^*_{Ib} across region Ib is therefore given for large r by

$$\Theta q^*_{\mathrm{Ib}}/(K_\ell \Delta T) = -\Theta \int_{-\infty}^{\xi} T^\ell_\phi \,\mathrm{d}\xi \sim c_0(\ln r + G(\Theta)). \tag{24}$$

Here $G(\Theta)$ is an arbitrary function of integration. As defined in (19), c_0 is the first-order approximation to the contact line temperature T_c.

Equation (24) shows that to leading order in r, the heat flow across region Ib is

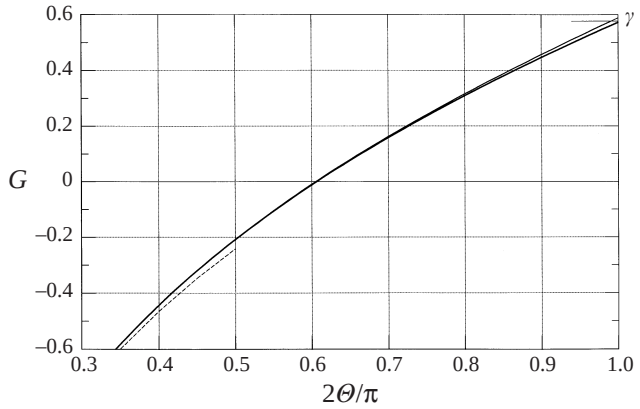

FIGURE 4. Function $G(\Theta)$ defined by (24). Broken curve, first term in (25*a*). Short horizontal line at $(2/\pi)\Theta = 1$, exact result (25*b*) for $\Theta = \pi/2$. Curves are computed from (25*a*): light curve, two terms; heavy curve, three terms.

proportional to the product $c_0 \ln r$ of the *local* temperature difference $T_{c*} - T_o$ and $\ln r$. The heat flow varies asymptotically as $\ln r$ since the solid is isothermal within region Ib, and the meniscus is asymptotically isothermal for large r. The arbitrary function of integration G has the following interpretation. The first term on the right of (24) is the heat flow from a solid at temperature c_0 to a liquid–vapour interface on which

$$T^{\ell v} = \begin{cases} c_0 & \text{if } r < 1, \\ 0 & \text{if } r > 1. \end{cases}$$

G is the difference between the heat flow across the actual meniscus, and the heat flow in this reference problem. This suggests that G will be positive or negative according as $T^{\ell v}$ varies on a length scale that is small or large compared with unity. The solution of (23) is needed to test this interpretation.

Problem (23) can be solved by finite differences, or by expressing T^{ℓ} as power series in the contact angle Θ. The power series has the advantage of giving a simple formula for $G(\Theta)$. Details for the three-term solution are given in Appendix A, and so is the exact solution for $\Theta = \pi/2$. The detailed variation of the heat flow within region Ib is given by equation (A 4) for the power series solution, and by (A 6) for the exact solution for $\Theta = \pi/2$. The discussion here emphasizes the behaviour of the total heat flow from this region, i.e. $G(\Theta)$ and its relation to $T^{\ell v}$. In Appendix A, it is shown that

$$G(\Theta) = \ln \Theta + \tfrac{1}{18}\Theta^2 - \tfrac{7}{2700}\Theta^4 + O(\Theta^6) \quad \text{for } \Theta \to 0, \text{ and that } G\left(\tfrac{1}{2}\pi\right) = \gamma. \quad (25a, b)$$

Here Euler's constant $\gamma = 0.5772\ldots$. For $\Theta = \pi/2$, (25*a*) predicts G to within 0.7% of the true value.

Figure 4 shows the function $G(\Theta)$. The figure shows that the three-term series (25*a*) gives G accurately for $0 < \Theta \leqslant \pi/2$. Solutions for two and three terms bracket the true value of $G(\pi/2)$. We note that G is an integral property of the solution: series for u and its derivatives converge more slowly, and are less suitable for calculation at larger values of Θ. The figure shows that $G < 0$ for small contact angles, but that $G > 0$ for Θ bigger than about one radian. The logic two paragraphs above suggests that $T^{\ell v}$ therefore varies from the contact line temperature to the saturation

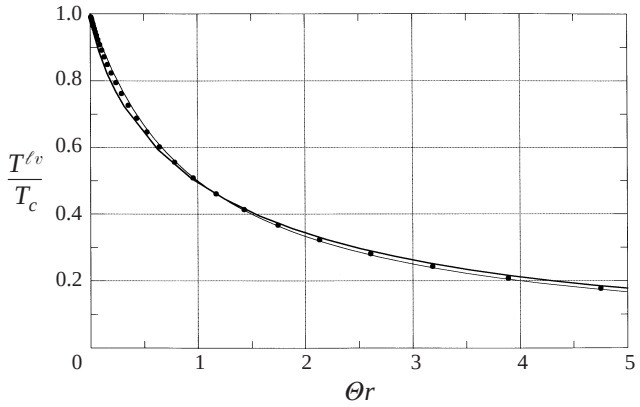

FIGURE 5. Meniscus temperature $T^{\ell v}/T_c$ calculated from (23) as a function of Θr. T_c is the contact line temperature. Heavy curve, exact solution (A 4) for $\Theta = \pi/2$; light curve, one-term solution (A 2) for $\Theta \to 0$; •, finite-difference solution of (23) for $\Theta = \pi/4$.

temperature on a scale large compared with unity for small Θ. Calculation of $T^{\ell v}$ confirms this expectation.

Figure 5 shows the normalized temperature $T^{\ell v}/c_0$ computed from (23) as a function of Θr for $\Theta \to 0$, $\Theta = \pi/4$ and $\Theta = \pi/2$. The ordinate is shown as $T^{\ell v}/T_c$ in the figure since $T_c = c_0 + O(k^{1/2})$. Symbols show values computed from (23) by finite differences. Curves show the elementary solutions derived in Appendix A. The figure shows that values of $T^{\ell v}$ for different Θ-values fall nearly on a single curve when plotted against Θr. This shows that $T^{\ell v}$ varies on a length scale L/Θ, which is large compared with L for $\Theta \to 0$. This result is consistent with the interpretation in the discussion of figure 4. The claim made about length scales in the paragraph following (2) is thus established.

8. Heat flow from the contact region

The heat flow from the contact region I is given by the composite expression formed from the expressions for regions Ia and Ib. The composite expression is constructed by adding the inner and outer equations (21) and (24), then subtracting their common part. The two solutions are matched for $\tilde{\xi} \to 0$ and $\xi \to \infty$. Correct to $O(k)$, the common part is $c_0 \ln r$. The dimensional heat flow q_i^* from the contact region is thus given by

$$\Theta q_i^*/(K_\ell \Delta T) = T_c \left(\frac{\sinh \alpha \tilde{\xi}}{\alpha \sqrt{k}} + G \right) + o(1). \tag{26}$$

This equation expresses the heat flow in terms of the contact line temperature $T_c = c_0(\mathscr{T}) + k^{1/2} c_1(\mathscr{T})$. The functions c_0 and c_1 are determined below in §9. As defined by (11), $\alpha = 1/\sqrt{\pi\Theta}$ and $\tilde{\xi} = \sqrt{k} \ln x$ as $r = x$ on the solid–liquid interface. $G(\Theta)$ is given by (25).

Equation (26) gives the heat flow from the contact region as the sum of two terms. The first accounts for the heat flow across the part of the meniscus on which $T^{\ell v} = 0$. The heat flow across that outer contact region varies nonlinearly with position r since $T^{s\ell}$ varies slowly with r. That heat flow vanishes as $r \to 1$, leaving the second term as a residue. That term gives the total heat flow occurring across the region Ib in which

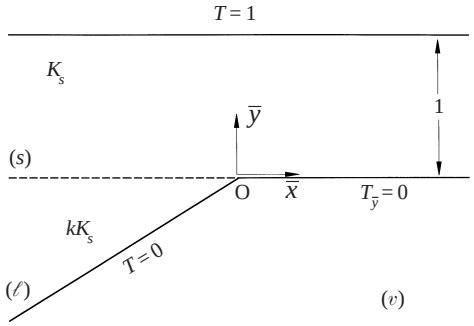

FIGURE 6. Definition sketch for the outer problem (9) incorporating the slab geometry.

$T^{\ell v}$ varies with position. Though (26) includes the total heat flow across the inner contact region, it does not describe the variation of heat flow within that region.

For applications, the overall effect of the contact region on the heat flow is needed. It is found by using (26) to evaluate the heat flow at fixed distance $\bar{r}$ from the contact line as $k \to 0$. This is equivalent to the outer limit defined in § 4, since $k \to 0$ in the limit $\mathscr{B} \to \infty$ with $\mathscr{T}$ fixed. This outer limit of (26) is found by using the identity $\tilde{\xi} = \mathscr{T} + \sqrt{k} \ln \bar{x}$ to express (26) in terms of the outer variable $\bar{x}$, and then using Taylor's theorem. The outer limit of (26) is thus

$$\Theta q_i^* / (K_\ell \Delta T) = T_c \left(\frac{\sinh \alpha \mathscr{T}}{\alpha \sqrt{k}} + \cosh \alpha \mathscr{T} \ln \bar{x} + G \right) + o(k). \tag{27}$$

$G(\Theta)$ is given by (25). Equation (27) holds if $|\ln \bar{x}| \ll \ln \mathscr{B}$.

Equation (27) has the following interpretation. The first term on the right side shows that at $O(k^{-1/2})$, the heat flow is asymptotically independent of position $\bar{r}$ as $k \to 0$ with $\bar{r}$ fixed. The solid therefore sees the contact line as a line heat sink. The second term shows that at $O(1)$, the outer heat flow varies as $\ln \bar{r}$. This is consistent with the general result (6) for the heat flow far from the contact line. Physically, both meniscus and solid are isothermal. The solid becomes isothermal at fixed $\bar{r}$ as its conductivity becomes infinite, and the meniscus becomes isothermal at fixed location since $K_l/h \ll d$. The heat flux thus varies as $\bar{x}^{-1}$ and the heat flow as $\ln \bar{x}$. Lastly, comparison of the coefficient of $\ln \bar{x}$ in (6) and (27) suggests correctly that $T_c \cosh \alpha \mathscr{T} = 1$ to leading order in k. This result is derived more systematically below.

9. Geometric effects: the solution in the outer region II

Figure 6 shows the geometry of the outer problem (9). Distances are measured in units of slab thickness, so the slab base is at $\bar{y} = 1$, as in (9*f*). The temperature on the vapour–liquid interface equals the saturation temperature at ∞. So $T^\ell = 0$, as in (9*e*). Solution of (9) is necessary to predict $c_0(\mathscr{T})$ and $c_1(\mathscr{T})$. The heat flow and contact line temperature T_c are then found from (26) and (19*b*).

By boundary condition (9*d*), the fluid–solid interface appears adiabatic to the solid to leading order in k. So T^s is uniform to leading order, and the outer solution has the form

$$T^s(\bar{x}, \bar{y}) = 1 + k^{1/2} \overline{T}_1 + O(k). \tag{28}$$

The contact line temperature T_c can now be found to leading order in k. Matching of the inner solution (20) for T^s to the outer solution (28) requires $c_0 = \operatorname{sech} \alpha \mathscr{T}$. By

k	$\mathscr{B}$	Θ	$\alpha\sqrt{k}$	$\alpha\mathscr{T}$
0.00217	2.08×10^5	0.344	0.0448	0.549

TABLE 3. Parameters for the conditions of Stephan & Busse's study.

(19*b*), $T_c = \operatorname{sech} \alpha\mathscr{T}$ to leading order. This result is identical to that given at the end of § 8. Since the outer temperature is uniform at leading order, T_c is asymptotically independent of slab geometry. If the substrate is not a slab, the dimension d in the definition of $\mathscr{B}$ is arbitrary to within a factor of order unity. To leading order in k, this does not affect the value of T_c : if d is increased by a numerical factor of order unity, $\mathscr{T}$ is unchanged to leading order in the small parameter k.

Next, we find $\overline{T}_1$ to estimate the error made if T_c is calculated from the formula above. By substitution of (28) into (9),

$$\overline{T}_{1\bar{x}\bar{x}} + \overline{T}_{1\bar{y}\bar{y}} = 0, \qquad \text{for } 0 < \bar{y} < 1 \quad \text{and} \quad -\infty < \bar{x} < \infty;$$
$$\text{for } \bar{x} \neq 0, \quad \overline{T}_{1\bar{y}}(\bar{x}, 0^+) = 0; \text{ on } \bar{y} = 1, \ \overline{T}_1 = 0. \tag{29a–c}$$

By (29*b*), the fluid–solid interface appears adiabatic to the solid, except at O. There, the outer solution sees a line heat sink, as discussed following (20). Formally, matching to the outer limit (20) of the inner temperature field requires $\overline{T}_1 \sim \alpha \tanh \alpha\mathscr{T} \ln \bar{r}$ as $\bar{r} \to 0$. The result for c_0 has been used here.

The solution of (29) is the Green's function for the slab. Let $q_1 = \alpha \tanh \alpha\mathscr{T}$, and $\bar{z} = \bar{x} + \mathrm{i}\bar{y}$ where $\mathrm{i} = \sqrt{-1}$. Also let Re denote the real part. Then $\overline{T}_1 = q_1 \operatorname{Re} \ln \tanh \frac{1}{4}\pi\bar{z}$. This satisfies (29*a*) for $\bar{r} \neq 0$, since $\ln \tanh \frac{1}{4}\pi\bar{z}$ is analytic in z for $0 < \bar{y} < 1$. Next, (29*c*) is satisfied. This follows by application of the identity $\ln f \equiv \ln |f| + \mathrm{i} \arg f$ to the function $f = \tanh \frac{1}{4}\pi\bar{z}$, and use of the result $|\tanh \frac{1}{4}\pi(x + \mathrm{i})| = 1$. Further, (29*b*) is satisfied since $\overline{T}_{1\bar{y}} = q_1 \frac{1}{2}\pi \operatorname{Re} \mathrm{i} \operatorname{cosech} \frac{1}{2}\pi\bar{z}$, and $\operatorname{cosech} \frac{1}{2}\pi\bar{z}$ is real on $\bar{y} = 0$. Lastly, the matching condition is satisfied. By (28), the outer temperature field in the solid is given by

$$T^s = 1 + k^{1/2} q_1 \operatorname{Re} \ln \tanh \tfrac{1}{4}\pi\bar{z} + O(k). \tag{30}$$

The correction term for T_c depends on $c_1(\mathscr{T})$. This function is found by matching, i.e. by equating the inner limit $\bar{z} \to 0$ of (30) to the outer limit (20) of the inner solution. So

$$c_1/c_0 = \alpha \ln \tfrac{1}{4}\pi \ \tanh \alpha\mathscr{T} \quad \text{where } c_0 = \operatorname{sech} \alpha\mathscr{T}. \tag{31}$$

Unlike c_0, c_1 is geometrically specific since the Green's function is domain-dependent.

10. Predicted heat flow and temperature

Definitions of the parameters are restated to make this section self-contained. The liquid–solid conductivity ratio $k = K_\ell/K_s$. The Biot number $\mathscr{B} = hd/K_\ell$: here d is the slab thickness and the heat transfer coefficient h is defined by (2). Next, $\mathscr{T} = \sqrt{k} \ln \mathscr{B}$ and $\alpha = 1/\sqrt{\pi\Theta}$, so $\alpha\mathscr{T} = \sqrt{k/(\pi\Theta)} \ln \mathscr{B}$. Lastly, the dimensional radius r_* is related to the dimensionless radii r and $\bar{r}$ by $r = \mathscr{B}\bar{r} = \mathscr{B} r_*/d$.

The predictions are compared with Stephan & Busse's results. Table 3 shows the

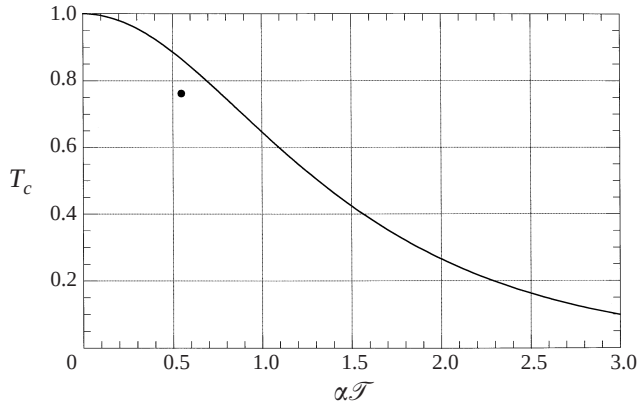

FIGURE 7. Dimensionless contact line temperature T_c as a function of $\alpha\mathscr{T}$. Curve, prediction (32); •, value calculated from results of Stephan & Busse (1992). See text for discussion.

parameters for the material properties given in their table 1, and the value of Θ computed by them. $\mathscr{B}$ is estimated for $d = 1\,\mathrm{mm}$.

10.1. *Contact line temperature* T_c

By (19) and (31),

$$T_c = (1 + \alpha k^{1/2} \ln \tfrac{1}{4}\pi \tanh \alpha\mathscr{T}) \operatorname{sech} \alpha\mathscr{T}, \tag{32}$$

for $k \to 0$ with $\mathscr{T}$ fixed. For the numbers in table 3, the error made by taking the second term in (32) as negligible is about 0.5%. So T_c is nearly independent of the solid geometry.

The dimensional contact line temperature T_{c*} is given by the first term of (32) as

$$\frac{T_{c*} - T_o}{T_w - T_o} = \operatorname{sech}\left(\sqrt{\frac{k}{\pi\Theta}} \ln \mathscr{B}\right). \tag{33}$$

The definitions of $\mathscr{T}$ and α have been used here. Physically, $T_{c*} \to T_w$ as $k \to 0$ since the solid is then perfectly conducting. Conversely $T_{c*} \to T_o$ as $h \to \infty$ since negligible superheat $T - T_o$ is then required to drive evaporation. Lastly, $T_{c*} \to T_o$ as $\Theta \to 0$ since the heat flux from the contact line increases with decreasing Θ. This formula allows us to assess whether the solid can be assumed isothermal or not in an application.

Figure 7 shows the relation (33) between $T_c = (T_{c*} - T_o)/\Delta T$ and $\alpha\mathscr{T} = \sqrt{k/(\pi\Theta)} \ln \mathscr{B}$. For the examples in table 2 of § 3, $\Theta = 0.3$, 0.4 and 0.7 radians. The corresponding values of $\alpha\mathscr{T}$ are 0.5, 0.3 and 1.4. The figure shows that T_c is close to the applied temperature in the first two cases. For the third case of water on stainless steel, T_c is about halfway between the applied and saturation temperatures, as stainless steel is a relatively poor conductor. Next, the symbol shows the result $T_c = 0.763$ of Stephan & Busse (1992). The value predicted by (32) is $T_c = 0.862$, which is about 13% higher than Stephan & Busse's result. Since their calculations are for a grooved solid, not a slab, the dimension d is arbitrary to within a factor of order unity. The prediction is insensitive to the choice made. Doubling d reduces the prediction by about 2% to $T_c = 0.848$. This example reinforces the conclusion reached above: for $k \to 0$, T_c is insensitive to geometry.

10.2. *Temperature within the solid*

The composite expression for T^s is constructed by adding the inner and outer solutions (19) and (30), then subtracting the common part $1 + q_1 \ln(\frac{1}{4}\pi\bar{r})$. Thus

$$T^s = T_c(1 + (\cosh\alpha\tilde{\xi} - 1)\,\mathscr{H}(\tilde{\xi})) + \alpha k^{1/2}\tanh\alpha\mathscr{T}\ \mathrm{Re}\ln\left(\frac{4}{\pi\bar{z}}\tanh\frac{\pi\bar{z}}{4}\right) + O(k). \quad (34)$$

Here T_c is given by (32). Throughout this work, $\bar{z} = \bar{x} + \mathrm{i}\bar{y}$ where the inner and outer coordinates are related by $z = \mathscr{B}\bar{z}$. Also $\tilde{\xi} = k^{1/2}\ln r$ and $\mathscr{H}(\tilde{\xi})$ is the Heaviside unit function.

The temperature T^{sf} on the solid–fluid interface $\bar{y} = 0$ is given by

$$T^{sf} = T_c\cosh(\alpha k^{1/2}\ln\ |\bar{x}|\mathscr{B}) + \alpha k^{1/2}\tanh\alpha\mathscr{T}\ \ln\left(\frac{4}{\pi\bar{x}}\tanh\frac{\pi\bar{x}}{4}\right) + O(k). \quad (35)$$

This expression holds for $\tilde{\xi} > 0$, i.e. for $|\bar{x}| > \mathscr{B}^{-1}$. For $|\bar{x}| < \mathscr{B}^{-1}$, $T = T_c$. The first term in (35) describes the solution in the contact region I. This term is independent of geometry. It is written in terms of the outer coordinate $\bar{x}$ for ease of use. The second term describes the modification of the temperature field by the boundary condition on the top of the slab. This term is geometrically specific.

The behaviour predicted for T^{sf} makes physical sense. First, T^{sf} becomes uniform as $k \to 0$ with $\bar{x}$ fixed. This follows because the argument of the first term is $\alpha\mathscr{T} + \alpha k^{1/2}\ln|\bar{x}|$ which approaches $\alpha\mathscr{T}$ as $k \to 0$. The first term in (35) thus approaches unity while the second term vanishes. Thus, $T^{sf} \to 1$ as $k \to 0$. Next, T^{sf} is an even function of $\bar{x}$ to $O(k^{1/2})$. The temperature distribution on the vapour–solid interface is thus identical with that on the liquid–solid interface at $O(k^{1/2})$. This prediction is geometrically specific. T^{sf} is symmetric about the contact line for the slab geometry because both interfaces are asymptotically adiabatic, and the solid is symmetric about the contact line. This prediction is confirmed by new finite-difference solutions in § 11. The heat flow and contact line temperature are independent of the outer geometry to leading order because they are determined by the solution for the contact region I. Lastly, T^{sf} decreases as $\alpha\mathscr{T}$ is increased at a fixed $x = \bar{x}\mathscr{B}$. Physically, the solid is cooled as h is increased with all else fixed. Mathematically, the second term in (35) is negative and becomes increasingly so as $\alpha\mathscr{T}$ is increased. The first term in (35) also decreases as $\alpha\mathscr{T}$ increases, since T_c decreases exponentially with increasing $\alpha\mathscr{T}$ by (32). T^{sf} therefore decreases with increasing $\alpha\mathscr{T}$.

Figure 8 shows $T^{s\ell}$ and $T^{\ell v}$ as functions of the inner coordinate $x = hx_*/K_\ell$ for the parameter values in table 3 above. Curve $T^{\ell v}$ is plotted from the small-Θ solution of (22). Curve $T^{s\ell}$ is plotted from the composite solution (35). Though the composite solution is used here, in effect the figure shows the contribution of the contact region to the temperature field: for the conditions of the figure, the outer (second) term in (35) is less than 0.5% of the inner (first) term. So it is meaningful to show Stephan & Busse's results for $T^{s\ell}$ here, though their solid is not a slab. The scatter in their results is an artefact of the replotting. Though Stephan & Busse also plot a quantity they call the interface temperature, their curve is misnamed. Comparison of their figure 5 with the corresponding figure 5.10 in Stephan (1992) shows that they plotted the local saturation temperature. For this work, $T^{\ell v}$ was therefore computed from the existing theory for the conditions given in Stephan & Busse (1992, table 1). Since the solid is isothermal near the contact line, the existing theory for an isothermal substrate was used here with ΔT set equal to the local temperature difference $T_{c*} - T_o$ given by them. The figure shows that both the conduction theory and Stephan & Busse's

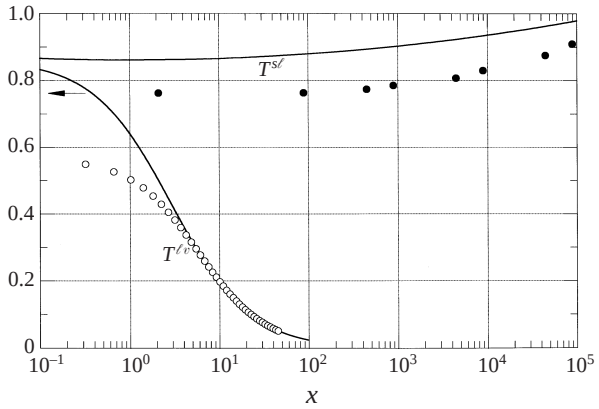

FIGURE 8. Dimensionless temperature T as a function of distance x from the contact line: $s\ell$, predicted temperature $T^{s\ell}$ on the solid–liquid interface; ℓv, predicted temperature $T^{\ell v}$ on the liquid–vapour interface; •, $T^{s\ell}$ replotted from Stephan & Busse (1992, figure 5). ○, $T^{\ell v}$ computed from the existing theory for the parameter values given in table of Stephan & Busse. See text for discussion.

simulation predict that $T^{s\ell}$ varies slowly with respect to $T^{\ell v}$ for the conditions of the simulation. The theory gives an interpretation of this result: $T^{s\ell}$ is slowly varying if the solid is highly conductive. The figure also shows that the theory predicts $T^{s\ell}$ with an error of at most 13%.

To replot Stephan & Busse's results, an origin must be chosen as the inclusion of the non-evaporating wetting film in that study makes the domain for the inner problem infinite, rather than semi-infinite, in x. This is shown in figure 1. For figure 8, their results were replotted by aligning the local maximum in $T^{\ell v}$ occurring in their results with the absolute maximum in $T^{\ell v}$ occurring at the contact line in the conduction theory. Their figure 4 verifies that the maximum occurs almost at the apparent contact line.

Lastly, the curves for $T^{s\ell}$ and $T^{\ell v}$ osculate at the contact line. The figure shows clearly that this happens in the conduction model. It is less clear from the figure that the computed values of $T^{\ell v}$ reach the common value shown by the arrow, for which the osculation in fact occurs. The apparent discrepancy is an artefact of the plotting. Since the origin for x is taken at the point of maximum heat flux, and the scale is logarithmic, $T^{\ell v}$ appears to asymptote to its value at the point of maximum flux.

10.3. *Heat flow*

The total dimensional rate q_* at which heat flows across the solid–liquid interface is given by (27), in which the contact line temperature T_c is now given by (32). Though (27) is derived for the contact region, it also gives the heat flow in the outer region to the accuracy quoted below in (36). In the language of asymptotic analysis, the inner expression (27) for the heat flow contains the outer expression to $O(k)$. This is because both $T^{\ell v}$ and $T^{s\ell}$ are asymptotically uniform at the outer edge of the inner region. The heat flux is thus asymptotically determined by conduction across a liquid wedge bounded by known isotherms. That is exactly the situation in the outer problem for the liquid. The heat flow is thus given by

$$\frac{\Theta q_*}{K_\ell \Delta T} = \frac{\tanh \alpha \mathscr{T}}{\alpha \sqrt{k}} + \ln \bar{x} + \ln \tfrac{1}{4}\pi \tanh^2 \alpha \mathscr{T} + G \operatorname{sech} \alpha \mathscr{T} + o(1). \tag{36}$$

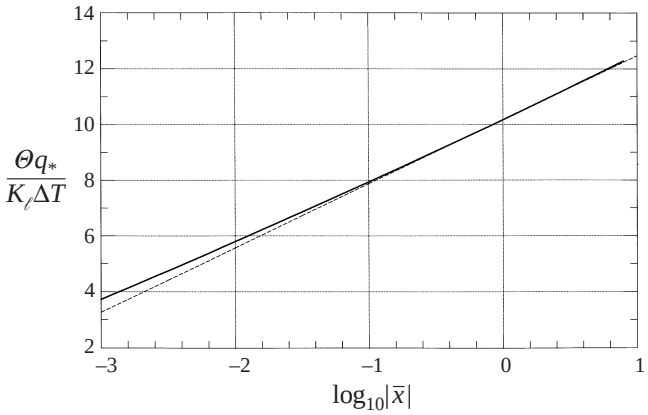

FIGURE 9. Heat flow across the strip of length $\bar{x} = x_*/d$ on the solid–liquid interface for the conditions in table 3. Solid curve, prediction (26) and (32) of the conduction model. Broken line, outer asymptote (36). See text for discussion.

Here $G(\Theta)$ is given by (25). Dimensionless variables are defined at the start of § 7. Like (27), from which it is derived, (36) holds if $|\ln \bar{x}| \ll \ln \mathscr{B}$.

This result shows how the evaporating meniscus affects the solid at the outer scale d. The heat flow is expressed as the sum of four terms. The first shows that to leading order in k, the solid sees a line heat sink at the contact line. The heat flow due to this term varies as the geometric mean conductivity $\sqrt{K_\ell K_s}$. So q_* is small compared with $K_s \Delta T$ as the liquid is a relatively poor conductor, but is large compared with $K_\ell \Delta T$ owing to the near-singularity at the contact line. The second term, varying as $\ln \bar{x}$, is the heat flow across a liquid wedge bounded by the isotherms $T = 1, 0$. The remaining terms are constant, and modify the strength of the leading-order sink. The first of these terms is negative, and the second is negative for sufficiently small Θ. Finite solid conductivity thus reduces slightly the strength of the line sink for small Θ. At fixed distance $\bar{x} \neq 0$ from the contact line, the solid therefore sees the heat flow due to the meniscus as the sum of a line heat sink, and a boundary flow varying as $\ln \bar{x}$.

Figure 9 illustrates this result with a numerical example. The figure shows the heat flow $\Theta q_*/(K_\ell \Delta T)$ across the strip of length $\bar{x}$ of the solid–liquid interface as a function of $\bar{x} = x_*/d$. The figure is drawn for the parameters given in table 3 above. The solid curve is calculated using (26) and (32), i.e. without taking the outer limit. The broken line is calculated from the outer equation (36). The figure shows that the broken line accurately fits the curve over about two decades in $\bar{x}$ centred on $|\bar{x}| = 1$. The fit is most accurate near $|\bar{x}| = 1$ since (36) is an outer representation of the heat flow. The figure also shows that at distances $\sim d$ from the contact line, $\Theta q_*/(K_\ell \Delta T) \gg 1$.

Equation (36) shows that the heat flow is asymptotically independent of the geometry of the solid for $k \to 0$. Of the four terms on the right of (36), only the third depends on the outer geometry through the numerical factor $\ln \pi/4$. This term becomes negligible as $k \to 0$. At a fixed distance from the contact line, the solid is asymptotically isothermal for $k \to 0$. The outer heat flow occurs from an isothermal solid, and is independent of the shape of the solid.

Next, (36) shows that at leading order in the small parameter k, the heat flow increases as $\alpha \mathscr{T} = \alpha \sqrt{k} \ln \mathscr{B}$ is increased with $\bar{x}$ fixed. In one sense, this behaviour is

d(mm)	$\tanh \alpha\mathscr{T}/(\alpha\sqrt{k})$	$\ln \bar{x}$	$\ln \frac{1}{4}\pi \tanh^2 \alpha\mathscr{T}$	$G\operatorname{sech} \alpha\mathscr{T}$	$\Theta q_*/(K_\ell \Delta T)$
1	11.2	−0.916	−0.060	−0.924	9.3
2	11.7	−1.61	−0.066	−0.910	9.1

TABLE 4. Elements of the heat flow prediction.

obvious since $\mathscr{B} = hd/K_\ell$, and increasing h must increase q_*. But it is less obvious that increasing d should increase the heat flow. This happens physically because (36) gives the heat flow across the meniscus to a fixed value of x_*/d. That heat flow increases with d. However, the formula does not imply that the heat flow across a meniscus in a channel of fixed width $2R$ should increase indefinitely with wall thickness d. In that geometry, the maximum dimension of the conduction domain is set by the meniscus radius R rather than the wall thickness d.

Table 4 shows the heat flow predicted for the conditions of Stephan & Busse's study, as given in table 3. In that study, the meniscus is a circular arc with contact angle Θ and so has finite extent. The results can be compared by estimating the maximum value of $\bar{x} = x_*/d$ possible in their geometry. From their figure 7, it can be seen that $x_* < 0.4\,\mathrm{mm}$: the dimensions given in their table 1 are needed here. This value was used to estimate $\bar{x}$ in table 4.

Stephan & Busse (1992, table 2) compute a dimensionless heat flow of 8.2. The table shows that (36) predicts a heat flow between 9.1 and 9.3. That is about 10% higher than the value computed by Stephan & Busse. The good agreement is due partially to cancellation of errors. To obtain table 4, we have used the conduction model of the contact region. We have also approximated the curved visible meniscus by a truncated linear meniscus, as described in the paragraph immediately above. It is shown below that the conduction model of the contact region under-estimates the heat flow from that inner region by about 10%. Since the estimates in table 4 exceed by about 10% the value of Stephan & Busse, replacement of a curved meniscus by a truncated linear meniscus introduces an error of order the difference, i.e. 20%. Even with this qualification, the comparison in table 4 suggests that the simple formula (36) can be used to estimate heat flows across the whole meniscus in applications.

This method works because the heat flow across the meniscus is dominated by the first term in (36), i.e. by the line sink. Table 4 shows that use of this term alone would lead to an over-estimate of the total heat flow by a factor of about 1.43. This suggests that for quick rough estimates, the relation $\Theta q_*/(K_\ell \Delta T) \sim (\tanh \alpha\mathscr{T})/(\alpha\sqrt{k})$ can be used. The corresponding dimensional heat flow is

$$q_* \doteqdot \sqrt{\frac{\pi}{\Theta} K_\ell K_s}\, \Delta T \tanh\left(\sqrt{\frac{k}{\pi\Theta}} \ln \mathscr{B}\right). \tag{37}$$

This can be a fair approximation to the total heat flow because $\bar{x}$ is not too different from unity anywhere on the visible meniscus, as the 5th column in table 4 shows.

10.4. *Heat flow within the contact region on an isothermal substrate*

This example is used to verify the phenomenological model. The comparison is made for the conditions of Stephan & Busse's calculation. For this work, the heat flow in the contact region was recomputed using their equations (3)–(5) and (7). For the conditions given in their table 1, specifically for $\Delta T = 1\,\mathrm{K}$, we find $\Theta = 0.332\,\mathrm{rad}$, i.e. 19.0°. This is about 3% less than the value of 0.344 rad reported by them.

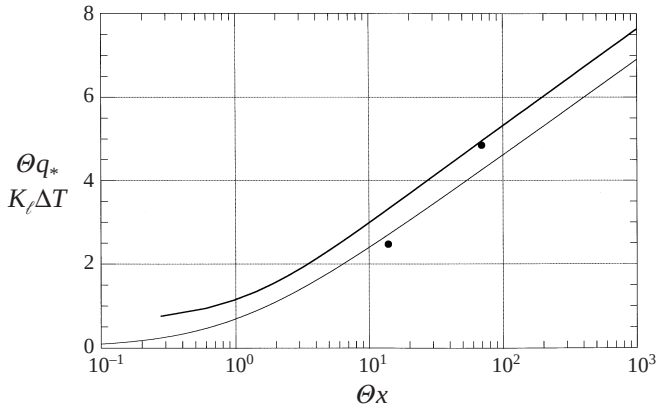

FIGURE 10. Heat flow across the strip of length x on the interface between the liquid and an isothermal substrate. Conditions are as in table 1 of Stephan & Busse: in particular $\Delta T = 1\,\mathrm{K}$, as in their contact region. Heavy curve, heat flow computed for this work from the existing theory. Light curve, conduction model. •, Values given by Stephan & Busse. See text for discussion.

Since the solid is taken as isothermal here, the phenomenological model reduces to the problem (23) describing the inner region Ib. Since it is assumed that $\Theta \to 0$ in the derivation of the existing theory, the heat flow for the conduction model is given by the first term in the power series for q_* given in Appendix A. Since both theories hold for $\Theta \to 0$, the comparison tests only the assumptions made in § 2 to derive the phenomenological model.

Figure 10 shows the dimensional heat flow q_* as a function of $x = hx_*/K_\ell$ for an isothermal substrate, i.e. for $\alpha\mathscr{T} = 0$. The heavy curve shows the heat flow computed for this work from the existing theory for the conditions given in table 1 of Stephan & Busse. The two points are the heat flows given by them for distances of 0.2 and $1\,\mu m$ from the contact line: these points are plotted using their value of Θ. The light curve is the prediction of the conduction model: this curve is plotted for the value of $\Theta = 0.332$ computed for this work. The figure shows that the conduction model under-estimates the heat flow, but that the error becomes small far from the contact line. For example, at $\Theta x = 100$, i.e. at about 1 μm from the apparent contact line, the conduction theory gives the heat flow with an error of about 10%. The percentage error would be even less at larger distances. The conduction model is therefore useful for applications.

11. Numerical tests of the solution of the conduction model

In the preceding section, it is shown that the assumptions made to derive the conduction model (4) lead to an error of around 10% in the heat flow for the conditions of Stephan & Busse's example. Here, the asymptotic analysis in §§ 4–7 is tested against finite-difference solutions of (4). The comparison shows that negligible error is made in practice by using the asymptotic analysis. The conclusion reached in § 10.4 is thus reinforced: the discrepancy between the new predictions and Stephan & Busse's results is due to the simplifying assumptions made to derive the conduction model.

Finite-difference solutions of (4) are easily obtained when the phase interface is isothermal, i.e. for $\alpha\mathscr{T} \to \infty$. Near the contact line, T then has the simple exact form (10) to within an unknown constant factor. The singularity can be removed by

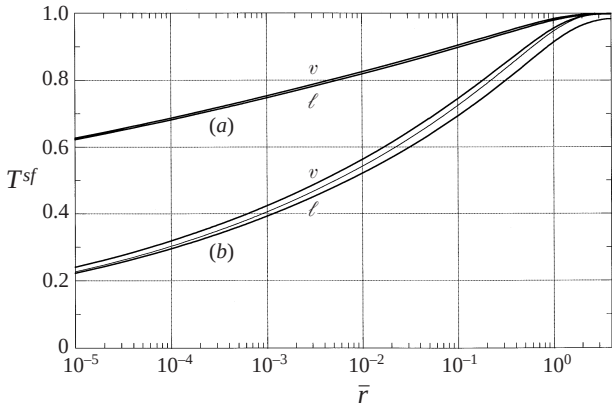

FIGURE 11. Temperature distribution predicted by the conduction model on the solid–vapour interface (curve v) and solid–liquid interface (curve ℓ) for contact angle $\Theta \to 0$ and an isothermal meniscus. (*a*) $\alpha\sqrt{k} = 0.040$, and (*b*) $\alpha\sqrt{k} = 0.126$. Heavy curves, finite difference solution of (B 1). Light curve, composite expression (38). See text for discussion.

the method in Appendix B. This method differs from that used in the heat transfer literature. There the singularity is treated by using many finite elements near the contact line. See, e.g. Stephan & Busse (1992) and Schonberg *et al.* (1995). The method used here could be extended to finite $\alpha\mathscr{T}$ by using the unnumbered equation displayed between (19) and (20) to remove the singularity.

For $\mathscr{T} \to \infty$, the phase interface is asymptotically isothermal at $T = 0$ because T_c is exponentially small in $\mathscr{T}$ by (32). On the solid–fluid interface the general result (35) reduces in the limit $\alpha\mathscr{T} \to \infty$ to

$$T^{sf} = \left(1 + \alpha k^{1/2} \ln \frac{\pi}{4}\right) |x|^{\alpha\sqrt{k}} + \alpha k^{1/2} \ln \left(\frac{4}{\pi\bar{x}} \tanh \frac{\pi\bar{x}}{4}\right) + O(k). \tag{38}$$

The identity $\lim_{A\to\infty} \operatorname{sech} A \cosh(A + B) = \exp B$ has been used here, with $A = \alpha\mathscr{T}$ and $B = \alpha\sqrt{k} \ln \mathscr{B}|x|$.

Figure 11 shows T^{sf} as a function of $\bar{x} = x_*/d$. Heavy curves are computed from finite-difference solutions of (4) for $\alpha\sqrt{k} = 0.126$ and 0.040. These values span the range of parameters in table 2. The figure shows that evaporative cooling of the liquid–solid interface makes $T^{s\ell}$ slightly less than T^{sv}. The difference is very small for the smaller value of $\alpha\sqrt{k}$. This is consistent with (38), which predicts T^{sf} to be asymptotically even in x. The figure also allows detailed comparison of (38) with the finite-difference solutions. The light curve for case (*b*) shows the prediction (38). Though k is not very small in this case, the figure shows that (38) closely predicts $T^{s\ell}$. The prediction for case (*a*) is not shown. It lies between the computed heavy curves for case (*a*), and would be invisible on the graph.

The approximations made in solving the conduction model (4) for large $\mathscr{B}$ therefore cause insignificant error for applications involving evaporation of non-metallic liquids from good conductors. So the discrepancy $\sim 10\%$ seen in the predictions of the inner temperature field on a conducting substrate in figures 7 and 8 must be due to the assumption of a separation of scales underlying (4). The size of that error is consistent with that seen in the inner heat flows in figure 10. It is also consistent with the estimates made in table 1 to assess the approximations underlying (4). Column 3 of table 1 shows that the change $\Delta\Theta$ in angle over the adjustment scale L is also

$\sim 10\%$ for the conditions of Stephan & Busse's simulation. This agreement with table 1 may be coincidental: as noted in the discussion of that table, scaling cannot show how small a dimensionless group should be for an approximation to hold.

The 10% error is also consistent with results in Stephan & Busse's figure 2. By integration of the heat flux distribution given there, it can be shown that about 10% of the total heat flow occurs in the region where Θ is established. The discrepancy between the two methods is thus due to the assumptions used to derive the conduction model, rather than to the approximations made to solve it.

12. Discussion

As the examples in the first paragraph of this paper show, the title problem occurs in several contexts. It is studied at present by either of two methods. In the heat pipe literature, the heat flow, film thickness and contact angle are predicted as part of the solution of a free-boundary problem. In the literature on thick evaporating films, Newton's law of cooling is used with a predicted heat transfer coefficient. That phenomenological approach is used, without justification, even when film rupture creates apparent contact lines: then, the existence of a contact angle is implicitly assumed, as in the studies by Anderson & Davis (1995), and Wilson *et al.* (1999). This paper unifies the two approaches by showing when a contact angle can be assumed and used with Newton's law of cooling.

Three main results are derived here. One is the derivation of the phenomenological model (4), together with conditions under which it holds. The other two are results for a specific boundary-value problem. First, it is shown that if the conditions (3) hold, all heat flow across the contact region occurs at dimensions large compared with those on which the apparent contact angle is established. A separation of scales then exists, and the contact angle can be introduced as a parameter. Under the same conditions, it is shown that Newton's law of cooling (2) holds with predicted heat transfer coefficient. In the heat pipe literature reviewed by Stephan & Busse (1992), the existence of a contact angle and a uniform interface temperature were assumed until recently. Substrate conduction was invoked to relax the contact line singularity. Stephan & Busse show numerically that in their example, that method over-estimates the heat flow by a factor of about 3.5. In § 10 above, it is shown that the present method predicts heat flows agreeing to within about 10% with those of Stephan & Busse. The older analyses fail because they assume a uniform interface temperature, not because they implicitly assume a separation of scales.

Next, the phenomenological model is used to solve the title problem in the limit $k \to 0$ of vanishing liquid–solid conductivity ratio: this limit is appropriate to the evaporation of non-metallic liquids from metals. The two main results are discussed in § 10. They are equation (33) for the dimensionless contact line temperature, and equation (36) for the heat flow. Those predictions are confirmed by comparison with both new and published solutions of the existing theory. It is shown that because the contact region contributes most of the heat flow, the equation given here for the heat flow across a linear phase interface can be used to estimate the total heat flow across the meniscus in Stephan & Busse's example, even though interface curvature is significant in their example.

Conditions for the validity of the phenomenological theory are found here by requiring the theory to be self-consistent. A subsequent work (Morris 2000) proves that the phenomenological theory is a limiting case of the existing theory of the evaporating wetting meniscus. Let H_s be the thickness of the non-evaporating wetting

film shown to the left of the contact line in figure 1. Then it is shown in the subsequent paper that in the limit $\beta = hH_s/K_l \to 0$, the existing theory has an inner-and-outer structure. The picture developed here describes the outer region: all the heat flow occurs here. The inner region in that analysis determines Θ, and the analysis gives a formula for Θ in terms of superheat ΔT. Together the two papers give a complete theory of the evaporating wetting meniscus holding if the thickness H_s of the non-evaporating wetting film is vanishingly small compared with the adjustment scale L, i.e. if $\beta \to 0$. The papers are presented in this way to emphasize that the heat flow is independent of wetting physics for $\beta \to 0$. Wetting physics then affects only the inner problem for Θ.

I would like to thank Peter Wayner and an anonymous referee for detailed helpful comments on this paper, and my former MS student Victor Moreno for discussions of the existing theory.

Appendix A. Solution of (23) for the heat flow and meniscus temperature

A.1. *Power series solution in* Θ^2

Let $\phi = \pi + \Theta\theta$ and $\rho = \Theta r$. In terms of these variables (23) is, without approximation

$$\left.\begin{aligned} &u_{\theta\theta} + \Theta^2 \rho (\rho u_\rho)_\rho = 0 \quad \text{for } 0 < \theta < 1; \\ &\text{on } \theta = 0,\ u = 1; \quad \text{on } \theta = 1,\ u_\theta + \rho u = 0. \end{aligned}\right\} \tag{A 1}$$

The solution of (A 1) can be expressed as the power series $u = u_0 + \Theta^2 u_1 + \Theta^4 u_2 + O(\Theta^6)$. The coefficients $u_0, \ldots$ depend only on ρ and the polar angle θ. They are determined by substituting the power series into (A1), and solving the resulting boundary-value problems for the coefficients. So

$$u_0 = 1 - \frac{\rho}{1+\rho}\theta,\ u_1 = \tfrac{1}{6}\rho \frac{1-\rho}{(1+\rho)^3}\left(\theta^3 - \frac{\rho+3}{\rho+1}\theta\right)$$

$$\text{and } u_2 = \tfrac{1}{36}B(\rho)\theta\left(\theta^2 - \frac{\rho+3}{\rho+1}\right) + \tfrac{1}{120}A(\rho)\theta\left(\frac{\rho+5}{\rho+1} - \theta^4\right). \tag{A 2}$$

Here

$$A(\rho) = \rho(1-\rho)(\rho^2 - 10\rho + 1)/(\rho+1)^5 \text{ and}$$

$$B(\rho) = \rho(3 - 38\rho + 42\rho^2 + 2\rho^3 - \rho^4)/(\rho+1)^6. \tag{A 3}$$

The heat flow in region Ib is given by $\Theta q^*_{\mathrm{Ib}}/(c_0 K_\ell \Delta T) = \ln(1+\rho) + q_1\Theta^2 + q_2\Theta^4 + O(\Theta^6)$. The coefficients $q_1 \ldots$ depend only on ρ. They are

$$q_1 = \tfrac{1}{18}\rho(\rho+3)^2/(1+\rho)^3 \text{ and}$$

$$q_2 = -\tfrac{1}{5400}\rho(14\rho^5 - 21\rho^4 - 240\rho^3 + 1330\rho^2 + 4410\rho - 1125)/(1+\rho)^6. \tag{A 4}$$

As $\rho \to \infty$, $\Theta q^*_{\mathrm{Ib}}/(c_0 K_\ell \Delta T) \sim \ln\rho + \frac{1}{18}\Theta^2 - \frac{7}{2700}\Theta^4 + O(\Theta^6)$. Comparison of this result with (24) gives (25). Figure 4 in the text shows that this method gives G accurately. The series for $T^{\ell v}$ converges less rapidly however, and for $\Theta > 1$ a finite-difference solution is preferable for that quantity.

A.2. *Exact solution for* $\Theta = \pi/2$

Liquid here occupies a quadrant in the (xOy)-plane. Problem (23) can thus be expressed as a Dirichlet problem for the variable $U(x, y) \equiv u_x - u$. That problem has an elementary solution for U, and u is then found by integration of an ordinary differential equation. Thus

$$u = 1 + \frac{2}{\pi}\left(y\mathrm{e}^{x}\int_{x}^{\infty}\frac{\mathrm{e}^{-s}}{y^2+s^2}\,\mathrm{d}s - \tan^{-1}\frac{y}{x}\right). \tag{A 5}$$

The flux across $y = 0$ is $-u_y|_{y=0} = (2/\pi)\mathrm{e}^{x}E_1(x)$ where $E_1(x) = \int_x^\infty \mathrm{e}^{-s}s^{-1}\,\mathrm{d}s$. By integration by parts, the heat flow across the strip between 0 and x is given by

$$q^*_{\mathrm{Ib}}/(c_0K_\ell\Delta T) = \frac{2}{\pi}\lim_{a\to 0}\int_a^x \mathrm{e}^{x}E_1(x)\,\mathrm{d}x = \frac{2}{\pi}(\mathrm{e}^{x}E_1(x) + \ln x + \gamma). \tag{A 6}$$

The identity $\lim_{a\to 0}\left(\mathrm{e}^{a}E_1(a) + \ln a\right) = -\gamma$ has been used. For it, see Abramowitz & Stegun (1965, equation 5.1.11). Comparison of (A 6) with (24) shows that $G(\pi/2) = \gamma$, since $\mathrm{e}^{x}E_1(x) = O(x^{-1})$ for $x \to \infty$.

Lastly, the meniscus temperature $T^{\ell v}$ is given by $T^{\ell v}/c_0 = (2/\pi)\int_0^\infty \mathrm{e}^{-ys}(1+s^2)^{-1}\,\mathrm{d}s$.

Appendix B. Treatment of the contact line singularity in finite difference solutions

Numerical analysis was used here to study cases in which Θ is small, and the interface temperature $T = 0$, i.e. $\mathscr{T} \to \infty$. The conduction equation for the liquid then simplifies to $T^\ell_{yy} = 0$. Thus the temperature gradient on the liquid side of the solid–liquid interface $T^\ell_y = -T^\ell(x,0)/\Theta x$. By (10), $T^\ell = O(x^p)$ for $x \to 0$. At the contact line $x = 0$, the flux T^ℓ_y is therefore infinite, but integrable.

T^s therefore satisfies

$$T^s_{xx} + T^s_{yy} = 0 \text{ for } 0 < y < 1;\ \text{for all } x,\ T^s(x,1) = 1;$$
$$\text{on } y = 0,\ T^s_y = \begin{cases} -\kappa T^s/x & \text{if } x \leqslant 0 \\ 0 & \text{if } x > 0. \end{cases} \tag{B 1}$$

Here $\kappa = k/\Theta$.

Problem (B 1) can be solved accurately even with a coarse grid by removing the singularity. Let p be the smallest positive root of $p\tan p\pi = \kappa$ and let $\overline{T} = r^p\cos p\phi$. $\overline{T}$ is the small-Θ limit of the separable solution (10). Also let c be an arbitrary constant. Without approximation, $t = T^s - c\overline{T}$ satisfies Laplace's equation with boundary conditions

$$t_x \sim -c\overline{T}_x \text{ as } |x| \to \infty;\ \text{for all } x,\ t(x,1) = 1 - c\overline{T}(x,1);\ \text{on } y = 0,$$
$$t_y = \begin{cases} -\kappa t/x & \text{if } x \leqslant 0 \\ 0 & \text{if } x > 0. \end{cases} \tag{B 2a, b, c}$$

Equation (B 2a) ensures that $T_x \to 0$ as $|x| \to \infty$. The problem for t was solved by finite differences on a uniform grid. c was found by plotting t on the solid–fluid interface, and choosing c visually so that the plot has no cusp at the origin. For the values of κ used for figure 11, the method gives $c = 0.992$.

REFERENCES

Abramowitz, M. & Stegun, I. A. 1965 *Handbook of Mathematical Functions*. Dover.

Anderson, D. M. & Davis, S. H. 1994 *J. Fluid Mech.* **268**, 231–265.

Anderson, D. M. & Davis, S. H. 1995 *Phys. Fluids* **7**, 248–265.

Bankoff, S. G. 1994 *Trans. ASME: J. Heat Transfer* **116**, 10–16.

Burelbach, J. P., Bankoff, S. G. & Davis, S. H. 1988 *J. Fluid Mech.* **195**, 463–494.

Cammenga, H. K. 1980 Evaporation mechanisms of liquids. In *Current Topics in Materials Science*, (ed. E. Kaldis), chap. 4. North-Holland.

Cook, R., Tung, C. Y. & Wayner, P. C. 1981 *Trans. ASME: J. Heat Transfer* **103**, 325–330.

DasGupta, S., Schonberg, J. A. & Wayner, P. C. 1993 *Trans. ASME*: *J. Heat Transfer* **115**, 201–208.

Grissom, W. M. & Wierum, F. A. 1981 *Intl J. Heat Mass Transfer* **24**, 261–271.

Guggenheim, E. A. 1967 *Thermodynamics*. North-Holland.

Mills, A. F. & Seban, R. A. 1967 *Intl J. Heat Mass Transfer* **10**, 1815–1827.

Moosman, S. & Homsy, G. M. 1980 *J. Colloid Interface Sci.* **73**, 212–223.

Morris, S. J. S. 2000 On the apparent contact angle between an evaporating meniscus and a superheated solid. *J. Fluid Mech.* (submitted).

Oron, A., Bankoff, S. G. & Davis, S. H. 1996 *Phys. Fluids* **8**, 3433–3435.

Potash, M. & Wayner, P. C. 1972 *Intl J. Heat Mass Transfer* **15**, 1851–1863.

Schonberg, J. A. & Wayner, P. C. 1992 *J. Thermophys. Heat Transfer* **6**, 128–134.

Schonberg, J. A., DasGupta, S. & Wayner, P. C. 1995 *Expl Therm. Fluid Sci.* **10**, 163–170.

Stephan, P. C. 1992 Wärmedurchgang bei Verdampfung aus Kapillarrillen in Wärmerohren. *Fortschr.-Ber. VDI Reihe* 19 Nr. 59. Dusseldorf: VDI.

Stephan, P. C. & Busse, C. A. 1992 *Intl J. Heat Mass Transfer* **35**, 383–391.

Wilson, S. K., Davis, S. H. & Bankoff, S. G. 1999 *J. Fluid Mech.* **391**, 1–27.